THEORETICAL AND NUMERICAL STUDIES OF THE AIR DAMPING OF MICRO-RESONATORS IN THE NON-CONTINUUM REGIME

A Thesis
Presented to
The Academic Faculty

by

Sarne M. Hutcherson

In Partial Fulfillment
of the Requirements for the Degree
Master of Science

G. W. Woodruff School of Mechanical Engineering
Georgia Institute of Technology
November 2004

THEORETICAL AND NUMERICAL STUDIES OF THE AIR DAMPING OF MICRO-RESONATORS IN THE NON-CONTINUUM REGIME

Approved by:

Dr. Wenjing Ye, Advisor
School of Mechanical Engineering
Georgia Institute of Technology

Dr. Jeffrey Streator
School of Mechanical Engineering
Georgia Institute of Technology

Dr. Farokh Ayazi
School of Electrical Engineering
Georgia Institute of Technology

Dr. Yogendra Joshi
School of Mechanical Engineering
Georgia Institute of Technology

Date Approved: November 2004

I dedicate this work to my parents, Michael and Debra Hutcherson, without whose love and unwavering support and encouragement I would not have made it this far.

ACKNOWLEDGEMENTS

I would like to thank my adviser, Dr. Wenjing Ye, for all of her help and guidance throughout my graduate study at Tech.

I would like to thank my committee members, Dr. Jeffrey Streator and Dr. Farokh Ayazi, for their questions and insights.

I would like to thank all those who encouraged and counseled me while I was choosing a graduate school, especially Dr. Patrick Mensah and Dr. Karen Crosby, and all those who have helped and supported me throughout my academic progression, with special thanks to Dr. Lovenia Deconge-Watson, Dr. Judy Perkins, and Dr. Diola Bagayoko.

I would like to thank the members of the GT BGSA for being my family away from home.

I would like to thank my parents, Michael and Debra Hutcherson, for being my model of strength, intelligence, and humility.

Finally, I would like to thank my Lord and Savior, Jesus Christ, for everything.

TABLE OF CONTENTS

LIST OF TABLES

LIST OF FIGURES

NOMENCLATURE

Symbol	Description
A	Area of the contact surface
A_0	Amplitude of device oscillation
a	Length of microbeam
	Length of the flow domain
	$G/2I$
b	Width of microbeam
	Width of the flow domain
	Body force
D	Damping work
d	Size of the gap between the resonator and electrode
	Distance between parallel surfaces
	Height of the constrained air column
	Depth of flow domain
	Thickness of the resonator
d_0	Distance between parallel plates
d_{gas}	Diameter of a gas molecule
dA	Area of the surface
dp	Momentum change
E_{Beam}	Energy input
ETM	Energy Transfer Model
$\mathbf{F}$	Force acting on the fluid
FMM	Free Molecular Model
f	Operating frequency
f_0	Non-dimensional damping force acting on plates in parallel motion
f_d	Total damping force acting on plates in parallel motion
G	Damping coefficient/ratio
g	Gravitational acceleration
h	Height of the constrained air column
Hz	Cycles per second
I	Moment of inertia
J	Polar moment of inertia
k	Boltzmann's constant
Kn	Knudsen number

Symbol	Description
L	Distance from the hinge of the vane to the contact area
	Peripheral length of the simulation domain
L_c	Characteristic length of the flow domain
ℓ	Distance the molecule travels under the beam
$\overline{\ell^2}$	Mean squared travel distance of molecule
u	Linear velocity of device normal to surface (plane of contact)
M	Molecular mass of gas molecule
	Particle momentum
	Mass of contact surface/wall
M_s	Mass of device
m	Mass of molecule/particle
m_p	Mass of particle
MB	Maxwell-Boltzmann gas velocity distribution function
MD	Molecular Dynamics
$MEMS$	Micro-Electro-Mechanical System(s)
MS	Maxwellian-Stream gas velocity distribution function
MU	Modified Maxwellian-Stream gas velocity distribution function
N	Number of molecules interacting with the contact surface
n	Number of moles
	Molecular density
N_A	Avogadro's Number; 6.022×10^{23} particles per mole
P	Pressure of gas
P_0	Environmental pressure
p	Pressure of gas
Q	Quality Factor
R	Universal gas constant; 8.314 J/mol/K
	Radial dimension of the disk
Re	Reynold's number
r	Radius of gyration
	Radial displacement
RF	Radio Frequency
T	Temperature of the gas
t	Time
$torr$	Unit of pressure; 1 torr = 133.3 Pa
U	Maximum velocity of the oscillating surface
u	Velocity of the fluid flow
	Linear velocity of contact area normal to the surface
V	Volume of the fluid
v	Linear velocity of particle normal to surface (plane of contact)
$\bar{v}$	Average velocity of gas molecule
v_r	Relative velocity of the gas molecule with respect to the surface
v_x	Average velocity of gas molecules
v_{x0}	Initial velocity of the molecule in the x-direction

Symbol	Description
v_{xi}	Velocity of the molecule in the direction normal to the contact surface
v_{yz0}	Initial velocity of the molecule in the yz-plane
w	Mass of oscillating vane
x	Flow direction
	Displacement of the device as it oscillates
β	Plate aspect ratio (length/width)
ΔE_{cycle}	Energy dissipation during one oscillation cycle of the device
ΔN	Number of collisions between a molecule and microbeam while the molecule travels under the microbeam
δ_{ij}	Kronecker Delta
ϵ	Ratio of the oscillation amplitude to the gap
ζ	Second coefficient of viscosity
η_{eff}	Effective fluid viscosity
Θ	Moment of inertia
θ	Angular displacement
$\dot{\theta}$	Angular velocity
$\ddot{\theta}$	Angular acceleration
κ	Ratio of gas molecule mass to wall mass
λ	Mean free path of a gas molecule
	Second coefficient of viscosity
μ	Viscosity of the fluid
ρ	Fluid density
ρ_{Si}	Density of silicon
ω	Natural frequency
σ	Squeeze number
τ	Product of natural frequency and time
τ_{ij}	Shear stress tensor of the fluid
ω	Natural frequency
	$\sqrt{G/2I}$ for $G \ll I$

SUMMARY

Micromechanical resonators are used in a variety of sensing and filtering applications. In these applications, the accurate performance of micro resonators depends on the sensitivity of these devices to a particular resonance frequency. This sensitivity is measured using the quality factor Q, which is the ratio of the total input energy into the device to the energy dissipated within a vibration cycle. A higher quality factor indicates a smaller resonance bandwidth, which makes the micro-resonator more effective in identifying a desired signal. It follows from the definition of the quality factor that higher Q values result from reductions in dissipation losses. To improve the design of these devices, it is important to know what factors contribute to the energy dissipation. Dissipation losses occur through damping by the ambient fluid, including viscous drag and squeeze-film damping, anchor losses for physically-fixed devices, thermoelastic damping, and other sources. The squeeze-film effect is of particular interest in micro-resonators as the fluid enclosed between the resonating components can provide significant dissipation.

This work covers investigations into the air damping of oscillating micromachined resonators that operate near a fixed wall, which is parallel to the oscillating surface. The main portion of this work focuses on the theoretical and numerical investigation of the air damping of micromachined resonators when the surrounding gas (air) is in the Free-Molecule regime. Errors and limitations of previous theoretical models have been found and corrected. A molecular dynamics simulation code that is suitable to handle a more general class of resonators has been developed. This code has been used to find the quality factor of a microbeam resonator. The results from the code were compared to existing experimental results, and were found to have very good agreement in the free molecular regime. The simulation was then used to investigate the effects of the oscillation mechanics on the behavior of the beam. The effects of the air gap-to-oscillation amplitude ratio, the oscillation frequency, and the ambient pressure were studied and their affect on the energy dissipation

and quality factor is presented.

The second part of this work focuses on the region between the bottom surface of a laterally-oscillating disk resonator and the substrate. The compressibility effects of a 1 micron thick film of air on a laterally-oscillating disk resonator were investigated. The pressure perturbation for this case was found to be minimal, which means that the compressibility effects of the fluid film will be negligible.

CHAPTER I

INTRODUCTION

1.1 Introduction to Micro-Electro-Mechanical Systems

Microelectromechanical, or MEMS, systems and devices have made a huge impact on the technology sector. These devices have allowed for the miniaturization of existing products, such as mobile phones, computers, and medical equipment, while also reducing cost and power requirements. MEMS have had a great impact on the inertial measurement, microfluidics, optics, pressure measurement, RF devices, and other markets [26, 7]. The applications of MEMS devices/systems in these markets include accelerometers, ink-jet printers, biolabs, optical switches and displays, microrelays, and sensors. Other examples include, but are not limited to, pressure sensors, inertial sensors and chemical sensors [20, 31, 36].

MEMS devices/systems are small systems of non-electrical components that have been fabricated using the same manufacturing techniques that are used to manufacture semiconductor electronics devices. Because of their size and the fabrication process, it becomes possible for these micro-mechanical systems to be built directly onto the same chips as the power and sensing circuity that operate them, adding the benefits that are associated with semiconductor production, i.e. batch fabrication. MEMS devices have an advantage over their macroscopic counterparts in their small size, greater sensitivity, and greater design flexibility. There are several classes of MEMS devices, but one of particular interest in the RF MEMS and communications arenas are the resonating devices. Resonating devices are used often in sensing applications.

1.2 Microresonators

Micromechanical resonators have been used extensively in a variety of sensing applications due to the high sensitivity of their resonance frequency to environmental parameters. They are also used in frequency filtration and stabilization. Due to their small size, they are able to

capture high frequency signals up to magnitudes of 10^9 Hz. Some common microresonators are beams (which includes cantilevers), disks, and comb-drives.

As with resonating devices, the accurate performance of micro resonators depends on the quality factor, Q, which reflects the resonance bandwidth and is the ratio of the total input energy into the device to the energy dissipated within a vibration cycle. A higher quality factor indicates a smaller resonance bandwidth, which makes the micro-resonator more effective in identifying a desired signal. A high quality factor is often desirable in order to achieve high sensitivity and high resolution. It follows from the definition of the quality factor that higher Q values result from reductions in dissipation losses. Dissipation losses occur through damping by the ambient fluid, including viscous drag if the device is oscillating laterally, and squeeze-film damping if the device is oscillating vertically, anchor losses for physically fixed devices, thermoelastic damping, and other sources. The squeeze-film effect is of particular interest in micro-resonators as the fluid enclosed between the resonating components can provide significant dissipation.

1.3 Motivation

The goal of this thesis is to provide an accurate model and approach to study the air damping of MEMS resonators in the non-continuum regime. There exists extensive studies of the air damping of devices by solving the Navier-Stokes Equations for the flow either analytically or numerically. Modeling the behavior of these devices in the non-continuum regime becomes difficult as the gas rarefaction effects begin to dominate. When these devices have very small, micron- and sub-micron scale feature sizes or they are operating in low pressure regions, the gas behavior can only be described based on the behavior of each individual molecule.

1.4 Scope of Study

This work covers investigations into the air damping of oscillating micromachined resonators. In particular, those resonators oscillating near a fixed wall, which is parallel to the oscillating surface. The main portion of this work focuses on the theoretical and numerical

investigation of the air damping of micromachined resonators when the surrounding gas (air) is in the *Free-Molecule* regime. Errors and limitations of previous theoretical models have been found and corrected. A molecular dynamics simulation code that is suitable to handle a more general class of resonators has been developed. This code has been used to find the quality factor of a microbeam resonator. The second part focuses on the region between the bottom surface of a laterally-oscillating disk resonator and the substrate.

1.5 Thesis Organization

This work is organized into 6 chapters. The first chapter provides an introduction to the work and some general background material. In Chapter 2, the underlying theories that govern this work are discussed in detail. This section includes a discussion on continuum as well as molecular damping theories. Chapter 3 looks at the use of molecular dynamics theory in the study of the air damping of resonating MEMS structures. Both analytical and numerical methods are reviewed and their applications and limitations are discussed. Chapter 4 presents comparisons between the theoretical and numerical results versus existing experimental data. Recommendations on the most accurate and robust methods are provided at the end of this chapter. Chapter 5 outlines the continuum study of the compressibility effects of a thin film on a laterally oscillating MEMS disk resonator. Contributions of gas interactions in the gap between the resonator and substrate are considered and the results are provided. Chapter 6 outlines the conclusions of this work and discusses future project possibilities.

CHAPTER II

AIR DAMPING

2.1 Introduction

There has been extensive research conducted in the past on the studies of different loss mechanisms and on the prediction of the quality factor of resonator devices [37, 5, 21, 19, 33, 24, 34]. Among different mechanisms that dissipate energy, viscous air damping has been shown to be a significant (and sometimes dominant) loss mechanism for devices operated in open air or in low vacuum [14]. In an experiment conducted by Zook *et al* [37], the measured quality factor of an oscillating microbeam decreases with the increasing pressure in the range of 10^{-2} torr to 10^{4} torr, indicating viscous air damping as the dominant loss mechanism within this pressure range. Accurate models and approaches for the prediction of air damping are therefore very important to the design of high-performance micro-resonators.

Most of the studies on air damping conducted in the past have employed continuum models [5, 34, 30]. These models are adequate for air in a device that has a minimum feature size on the order of microns or larger and is operated at either the atmospheric pressure or a pressure that is slightly below the atmospheric pressure. Some examples for such devices are accelerometers and gyroscopes. However, there are cases in which continuum theory may fail to give a good prediction, for example, micro-scale/nano-scale resonators operated in a low vacuum [37] or nano-scale devices operated at the atmospheric pressure. A common feature of air in these examples is that gas rarefaction effects are so significant that the interaction between each molecule[1] with moving structures must be accounted for individually in order to obtain an accurate prediction of the fluid effects on the oscillating devices.

[1]The terms *molecule* and *particle* are used interchangeably throughout this thesis.

The parameter that determines the degree of rarefaction and the degree of validity of the continuum model [8] is the Knudsen number (Kn) which is defined as the ratio of the mean free path of the gas molecule to the characteristic length of the flow. According to the definition of Knudsen number,

$$Kn = \frac{\lambda}{L_c} = \frac{RT}{\pi\sqrt{2}d_{gas}^2 N_A P L_c}, \tag{1}$$

where λ is the mean free path of the gas, L_c is the characteristic length of the domain, d_{gas} is the diameter of the gas molecule, and N_A is Avogadro's number. The Knudsen number defines the different air flow regimes, which are summarized in Table 1 [25] and shown in Figure 1 for various characteristic lengths. In the *Continuum Regime*, the Navier-Stokes

Table 1: Air Flow Regimes

Continuum Regime	$Kn \leq 10^{-3}$
Slip Regime	$10^{-3} \leq Kn \leq 10^{-1}$
Transition Regime	$10^{-1} \leq Kn \leq 10$
Free-Molecule Regime	$Kn > 10$

equations with no-slip boundary conditions can be used to determine fluid flow behavior. No-slip boundary conditions apply in this regime because the velocity of the surface contacting the fluid has an immediate and direct influence on the velocity of the fluid. For the *Slip Regime*, the Navier-Stokes equations can also be used, but slip boundary conditions are necessary because as the ratio between the mean free path and the characteristic length increases, it becomes possible that the velocity of the fluid at the contact surface may not be the same as the velocity of the surface, or there may be a delay in response of the motion of the fluid to the motion of the surface. The *Transition Regime* marks the transition from continuum mechanics to molecular dynamics. In this regime, the number of intermolecular collisions is small and not significant enough to be randomly canceled out and, thus, the collisions of each individual molecule must be taken into account. In the *Free-Molecule Regime*, there are almost no interactions between the molecules of the fluid (gas). In this regime, intermolecular collisions can often be neglected as collisions between air molecules

with the device's surfaces dominate the gas transport. In this regime, the velocity distribution of molecules in a general gas assembly under equilibrium conditions has been shown to follow the Maxwell-Boltzmann (MB) gas velocity distribution. For micro-resonators with gap size of 1μm and operated at a pressure of 5 torr or less, the Knudsen number of the surrounding air is 10 or higher. According to Table 1 listed above, air in these devices is in the free-molecule regime. Figure 1 shows the Knudsen numbers for varying characteristic

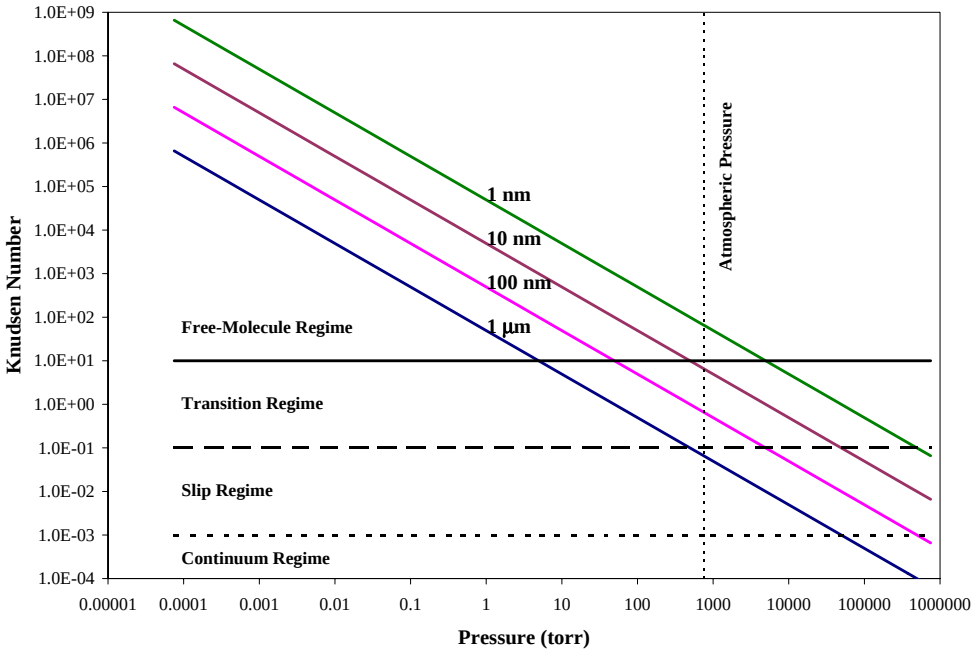

Figure 1: Knudsen Numbers for Various Characteristic Lengths

lengths and a constant temperature of 273 K. The horizontal lines represent the transitions between the flow regimes, as shown in Table 1. For example, a device having a characteristic length of 1μm will be operating in the free molecular regime for a pressure lower than 1 torr. For this same device operating at or around atmospheric pressure (about 760 torr), the flow will be between the slip and transition regimes.

Micromechanical devices are much more sensitive to environmental conditions than conventional machines. There performance is effected not only by their geometry and mechanical constraints, but also by external factors such as local pressure and temperature. In MEMS devices, air damping can play a significant role in the efficiency of the device. It is

because of this that it is important to analyze the operating environment and evaluate any conditions that will effect device performance. In the case of air damping, local pressure and temperature will have a significant effect. Assuming that air behaves as an ideal gas, its macroscopic properties (i.e. density and viscosity) can be directly derived from its pressure and temperature. These macroscopic properties determine how the device will behave in its environment. In Section 2.2.1, the effects of the environmental state are discussed. Section 2.3.1 highlights fluids dynamics theories that apply directly to the analysis of MEMS devices. As the operating pressure decreases or the device size is on the order of micro- or nano-meters, continuum theory begins to lose its validity. As the gas surrounding the device becomes rarefied, analysis must move away from the macroscopic quantities and focus on the individual interactions between gas molecules and the device. It is for these cases that molecular dynamics theory becomes important. Section 2.2.2 describes some generally accepted molecular dynamics theory, while Section 2.3.2 provides a thorough examination of the two analytical methods that are most applicable to these free-molecular cases.

2.2 Theory

2.2.1 Continuum Theory

To determine the energy transfer between a resonator and the gas that surrounds it, the dynamic properties of the fluid must be considered. When working with fluids in the continuum region it is important to determine whether the flow of the fluid is *incompressible* or *compressible*. Incompressible flows generally refer to liquids because they are highly resistive to compression, tending to maintain their density with changes in temperature or pressure. Compressible flows generally refer to gases because their densities fluctuate readily with changes in temperature and pressure.

2.2.1.1 Continuum Mechanics

A Newtonian fluid is a fluid in which the relationship between shear stress and shear strain rate is linear. This relationship is expressed in the form of Stokes' Law,

$$\tau_{ij} = \mu \left(\frac{\partial u_j}{\partial x_i} + \frac{\partial u_i}{\partial y_j} - \frac{2}{3} \frac{\partial u_m}{\partial x_m} \delta_{ij} \right),$$

where τ_{ij} is the shear stress tensor, u is the velocity of the flow, μ is the fluid viscosity, and δ_{ij} is the Kronecker Delta. For a viscous Newtonian fluid, the generalized Navier-Stokes equation is

$$\rho\left(\frac{\partial u_i}{\partial t}+u_j\frac{\partial u_i}{\partial x_j}\right)=-\frac{\partial P}{\partial x_i}+b_i+\frac{\partial}{\partial x_j}\left[\mu\left(\frac{\partial u_i}{\partial x_j}+\frac{\partial u_j}{\partial x_i}-\frac{2}{3}\delta_{ij}\frac{\partial u_k}{\partial x_k}\right)\right]+\frac{\partial}{\partial x_i}\left(\zeta\frac{\partial u_k}{\partial x_k}\right), \quad (2)$$

where ρ is the fluid density, P is the pressure, b is the body force, u is the fluid flow velocity, x is the flow direction, and ζ is a second coefficient of viscosity, $\zeta=\lambda+\frac{2}{3}\mu$ (λ is another second coefficient of viscosity), which is zero for a monoatomic gas [15]. The Navier-Stokes equation describes the motion of the fluid in terms of Newton's Law for Fluids,

$$\frac{\mathbf{F}}{V}=\rho\frac{\partial \mathbf{u}}{\partial t}+\rho\mathbf{u}\cdot\nabla\mathbf{u}, \quad (3)$$

where $\mathbf{F}/V$ can include the viscous ($\mu\nabla^2\mathbf{u}$), pressure ($-\nabla P$), and body ($\mathbf{b}$) forces acting on the fluid. There are several assumptions and boundary conditions that can be used to reduce the Navier-Stokes equations . Table 2 lists reduced forms of these equations for *Irrotational, Incompressible* and *Steady Incompressible* flows. When applying any of

Table 2: Reduced Forms of the Navier-Stokes Equations [32]

Flow Description	**Reduced Navier-Stokes Equation**
Irrotational, Incompressible Flow with $\mathbf{b}=\mathbf{0}$	$\rho\frac{\partial u}{\partial t}+\rho\mathbf{u}\cdot\nabla\mathbf{u}=-\nabla P+\mu\nabla^2\mathbf{u}$
Low Reynolds Number	$\rho\frac{\partial u}{\partial t}+\nabla P=\mu\nabla^2\mathbf{u}$
Low Reynolds Number and Low Pressure	$\rho\frac{\partial u}{\partial t}=\mu\nabla^2\mathbf{u}$
High Reynolds Number	$\rho\frac{\partial u}{\partial t}+\rho\mathbf{u}\cdot\nabla\mathbf{u}=-\nabla P$
No Pressure Force	$\rho\frac{\partial u}{\partial t}+\rho\mathbf{u}\cdot\nabla\mathbf{u}=\mu\nabla^2\mathbf{u}$
Steady Incompressible Flow	$\frac{\partial u}{\partial t}=0$
Low Reynolds Number	$\nabla P=\mu\nabla^2\mathbf{u}$
Low Reynolds Number and Low Pressure	$\nabla^2\mathbf{u}=0$
High Reynolds Number	$\rho\mathbf{u}\cdot\nabla\mathbf{u}=-\nabla P$
Small Pressure Forces	$\rho\mathbf{u}\cdot\nabla\mathbf{u}=\mu\nabla^2\mathbf{u}$

these forms of the Navier-Stokes equations, it is necessary to choose accurate boundary conditions. For the continuum regime ($Kn \leq 0.001$), no-slip boundary conditions must be used, that is the velocity of the fluid along the solid-fluid interface must be equal to the velocity of the solid, or $u(x_s, y_s, z_s, t) = U(x_s, y_s, z_s, t)$, where u and U are, respectively, the fluid and solid velocities at the solid-fluid interface and x_s, y_s, and z_s are the coordinates of the solid surface. For the slip regime ($0.1 \geq Kn > 0.001$), slip boundary conditions must be used. These can take many forms, with varying order, and are not discussed in detail in this paper.

2.2.1.2 Squeeze-Film Damping

When the device's surface is parallel to a nearby wall (electrode or substrate) and its motion is toward that wall, the phenomenon of *squeeze-film damping* can occur. Squeeze-film damping results when a pressure difference develops between the gap and the environment. When the device moves close to the wall, the air film in the gap is squeezed and a positive differential pressure develops in the gap as the pressure inside the gas increases and the gas is squeezed out of the gap. When the device moves away from the wall, the gas is drawn into the gap, decreasing the pressure of the gas in the gap and causing a negative differential pressure. For one-dimensional flow cases, the damping of the device is inversely proportional to the gap size, i.e. the smaller the gap, the greater the resulting damping force. In the continuum regime, the flow behavior can be obtained form the Navier-Stokes

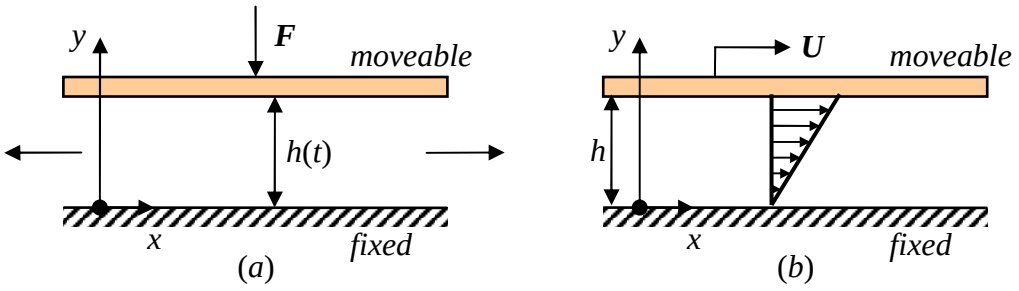

Figure 2: Common air damping mechanisms in MEMS devices: (a) Squeeze-Film Damping and (b) Slide-Film Damping

equations with body force terms equal to zero ($\mathbf{b} = 0$).

2.2.1.3 Slide-Film Damping

Slide-film damping occurs when the device's surface is parallel to a nearby wall and its motion is also parallel to that wall[2]. The resulting flow from this motion is similar to Couette flow (Figures 3(a) & 3(c)) in most cases. For Couette flow, the viscous force determines the behavior of the fluid. When the inertial force effects become comparable to

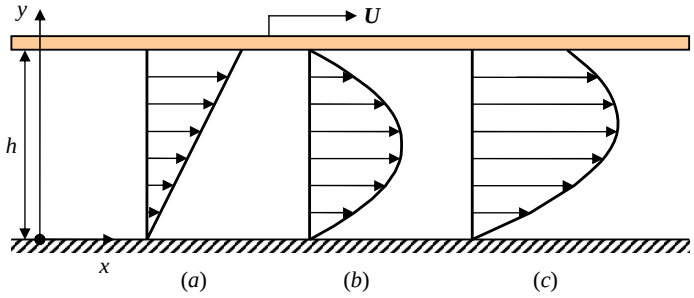

Figure 3: Velocity Profiles for Fluid Flows: (a) simple Couette flow ($\Delta P = 0$, $U \neq 0$), (b) Poiseuille flow ($\Delta P \neq 0$, $U = 0$), and (c) general Couette flow (linear combination of flows (a) and (b))

the viscous force effects, the slide-film damping can also take the form of stokes flow. For more general cases in the continuum regime, the Navier-Stokes equations can be used to determine the behavior of the flow.

2.2.2 Molecular Damping Analysis

In the case of molecular damping, the fundamental damping mechanism is the momentum and energy exchange between the molecules and devices. Using the shaded wall in (Figure 4) [13]as a reference, the behavior of one molecule can be studied. The molecule is assumed to be monoatomic hard sphere and will be referred to as a particle in the rest of this section. If a particle of mass m and velocity v strikes the wall, only the x-component of its velocity will change, assuming that the collision between the particle and the wall is specular and the walls roughness is negligible. Thus, the only change in the particle's momentum that will occur will be in the x-direction. The change in momentum (ΔM) of the particle will be

$$\Delta M = (-mv_x) - (mv_x) = -2mv_x = -2mv\cos\theta,$$

where θ is the angle between the velocity vector v and the normal to the shaded wall. The

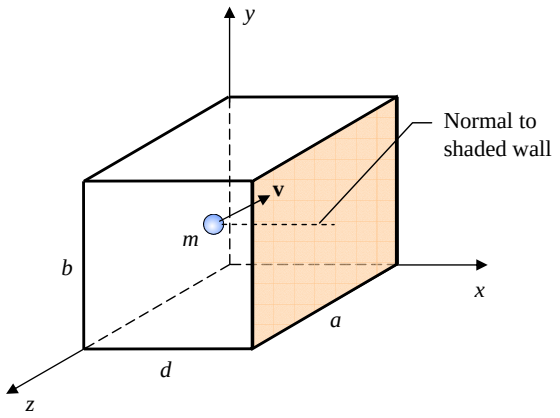

Figure 4: A box of length a, width b, and depth d. There is a molecule of mass m traveling with velocity v colliding with the walls of the box.

impulse delivered to the wall will be $+2mv\cos\theta$. In an enclosed area, this molecule will strike the wall repeatedly. The time Δt required for the molecule to travel to the opposite end of the cube and back again can be used to calculate the average rate of change of momentum. For this single molecule,

$$\frac{\Delta M}{\Delta t} = \frac{2mv_x}{2d/v_x} = \frac{mv_x^2}{d},$$

where d is the distance from the shaded wall to the opposite wall. From Newton's Second Law, $F = dM/dt$, the rate at which momentum is delivered to the wall is the force acting on that wall. By adding up the contributions of all of the molecules that strike the wall, the total force can be found. Dividing the total force F_x by the area (A) of the wall then gives the pressure P on that wall,

$$P = \frac{F_x}{A} = \frac{mv_{x1}^2/d + mv_{x2}^2/d + mv_{x3}^2/d + \ldots + mv_{xN}^2/d}{A},$$

where v_{xi} is the velocity of each particle and N is the number of molecules inside the enclosed volume ($N = \rho V$). For the case of a cubic volume ($a = b = d = L$), the pressure becomes

$$\begin{aligned} P &= \frac{mv_{x1}^2/L + mv_{x2}^2/L + mv_{x3}^2/L + \ldots + mv_{xN}^2/L}{L^2} \\ &= \frac{m}{L^3}\left(v_{x1}^2 + v_{x2}^2 + v_{x3}^2 + \ldots + v_{xN}^2\right) = \frac{mN}{L^3}\bar{v}_x^2 = \frac{nmN_A}{V}\bar{v}_x^2, \end{aligned}$$

where $\overline{v_x^2}$ is the mean square velocity of the gas molecules, V is the volume, n is the number of moles, and N_A is Avogadro's number. Again, this equation results from the assumptions that the volume is enclosed and is cubic and that all walls of the volume are stationary.

If the wall is in motion, the particle will not only experience a change in momentum, but also a change in the magnitude of its velocity (and thus its energy), depending on the velocity of the wall. Using the laws of conservation of kinetic energy (4) and conservation of linear momentum (5), it can be shown that the increase or decrease in the velocity of the molecule after colliding with the moving surface will be $2u$, where u is the velocity of the moving surface normal to the surface. Considering the collisions between a wall of mass

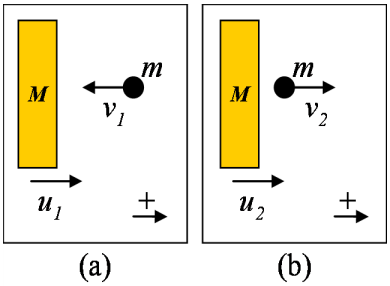

Figure 5: Diagram of Head-On Collision Model: (a) Before Collision, (b) After Collision

M and a gas particle of mass m, the velocity increment can be found by solving equations (4) and (5) for the unknowns u_2 and v_2, which are the velocities after a head-on-collision between the surface and particle, respectively.

$$\begin{aligned} Mu_1 - mv_1 &= Mu_2 + mv_2 \qquad (4) \\ \kappa = \frac{m}{M} \Rightarrow u_1 - \kappa v_1 &= u_2 + \kappa v_2 \\ (u_1 - \kappa v_1)^2 &= (u_2 + \kappa v_2)^2 \\ u_1^2 - 2\kappa u_1 v_1 + v_1^2 &= u_2^2 + 2\kappa u_2 v_2 + v_2^2 \end{aligned}$$

$$\begin{aligned} Mu_1^2 + mv_1^2 &= Mu_2^2 + mv_2^2 \qquad (5) \\ u_1^2 + \kappa v_1^2 &= u_2^2 + \kappa v_2^2 \end{aligned}$$

Subtracting equation (5) from (4) yields equation (6)

$$u_1^2 - 2\kappa u_1 v_1 + \kappa^2 v_1^2 = u_2^2 + 2\kappa u_2 v_2 + \kappa^2 v_2^2$$
$$u_1^2 + \kappa v_1^2 = u_2^2 + \kappa v_2^2$$
$$-2\kappa u_1 v_1 + \left(\kappa^2 - \kappa\right) v_1^2 = 2\kappa u_2 v_2 + \left(\kappa^2 - \kappa\right) v_2^2$$
$$-2u_1 v_1 + \left(\kappa - 1\right) v_1^2 = 2u_2 v_2 + \left(\kappa - 1\right) v_2^2$$
$$0 = \left(\kappa - 1\right) v_2^2 + \left(2u_2\right) v_2 + \left(2u_1 v_1 - \left(\kappa - 1\right) v_1^2\right)$$

$$\begin{aligned} v_2 &= \frac{-\left(2u_2\right) \pm \sqrt{\left(2u_2\right)^2 - 4\left(\kappa - 1\right)\left(2u_1 v_1 - \left(\kappa - 1\right) v_1^2\right)}}{2\left(\kappa - 1\right)} \\ &= \frac{-u_2 \pm \sqrt{u_2^2 - 2\kappa u_1 v_1 - \kappa\left(\kappa - 1\right) v_1^2 + 2u_1 v_1 - \left(\kappa - 1\right) v_1^2}}{\left(\kappa - 1\right)} \end{aligned}$$

Since $M \gg m$, then $\kappa \to 0$ and $u_2 \approx u_1$. This allows for the estimation of v_2 by equation (6).

$$\begin{aligned} \lim_{\kappa \to 0} \lim_{u_2 \approx u_1} v_2 &= \frac{-u_1 \pm \sqrt{u_1^2 + 2u_1 v_1 + v_1^2}}{(-1)} = \frac{-u_1 \pm \left(u_1 + v_1\right)}{-1} \\ v_2 &= v_1 + 2u_1 \end{aligned} \tag{6}$$

When the wall is moving in the same direction as the molecule, the molecule's velocity after the collision is given as $v_2 = v_1 - 2u_1$. If the velocity of the wall varies with time, the velocity of the particle after colliding with the wall can be generalized as $v = v_0 - 2u(t)$. By using this relation, the rate of momentum transfer and the change in kinetic energy of the molecule can be used to determine the pressure acting on the wall and the energy transferred into the gas system from the moving wall.

2.3 Review

2.3.1 Continuum Theory

2.3.1.1 Squeeze-Film Damping

For continuum cases, the squeeze-film damping of two plates can be determined using solutions to variations of the Navier-Stokes equations. The most common of these variations is the linearized isothermal Reynolds equation for compressible gas films equation (7) [29],

$$\frac{P_0 d_0^2}{12\eta_{eff}} \nabla^2 \left(\frac{p(x,y,t)}{P_0}\right) - \frac{\partial}{\partial t}\left(\frac{p(x,y,t)}{P_0}\right) = \frac{\partial}{\partial t}\left(\frac{z}{d_0}\right), \tag{7}$$

where P_0 is the environmental pressure, p is the dimension- and time-dependent pressure perturbation, η_{eff} is the effective viscosity and is a function of the Knudsen number, d_0 is the distance (gap) between the parallel plates, and z is the variation in the gap size.

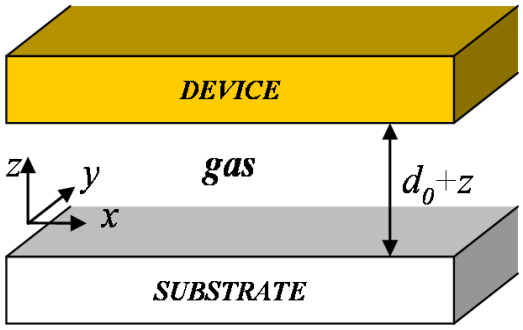

Figure 6: Domain of the linearized isothermal Reynolds equation for compressible gas films

In his work on isothermal squeeze films [4], Blech provides an estimation of the damping force acting on parallel plates, based on a linearized form of the Reynolds equation. Blech shows that for the case of an oscillating plate, there are spring and damping forces that will act on the plates due to the squeezing and stretching of the gas film. The non-dimensionalized damping force acting on rectangular plates in parallel motion is given as equation (8)

$$f_0 = \frac{64\sigma\epsilon}{\pi^6} \sum_{m,n\ odd} \frac{m^2 + (n/\beta)^2}{(mn)^2 \left\{ [m^2 + (n/\beta)^2]^2 + \sigma^2/\pi^4 \right\}}, \tag{8}$$

where σ is the squeeze film number equation (9), ϵ is the ratio of the oscillation amplitude to the gap (A_0/d_0), and β is the plate aspect ratio (l/w). The squeeze number provides an indication of how strongly the viscous forces affect the damping.

$$\sigma = \frac{12\mu l^2 \omega}{P_0 d_0^2}, \tag{9}$$

where μ is the viscosity, ω is the oscillation frequency, P_0 is the environmental pressure, and d_0 the height of the constrained air column. It has been shown in the literature [35, 17, 28] that when σ is small, the gas behaves like an incompressible fluid, and viscous damping effects dominate. Alternately, when σ is large, spring forces dominate and the gas acts like a spring resulting in much smaller energy dissipation. The total damping force f_d is defined

as $f_d = f_0 \cos(\tau) P_0 A$, where A is the area of the rectangular plate $(l \cdot w)$ and $\tau = \omega t$. The damping work done by this damping force within a period of the plate's oscillation is given by

$$\begin{aligned} D &= \int_0^T f_d \cdot \dot{x} dt = f_0 P_0 A \omega A_0 \int_0^T \cos^2(\tau) dt \\ D &= \pi f_0 P_0 A A_0 \\ D &= \pi \frac{64 P_0 A A_0^2}{\pi^5 d_0} \sum_{m,n\ odd} \frac{\sigma \left[m^2 + (n/\beta)^2\right]}{(mn)^2 \left\{\left[m^2 + (n/\beta)^2\right]^2 + \sigma^2/\pi^4\right\}} \end{aligned}$$

The quality factor for a beam characterized by these parallel plates will be

$$Q = \frac{2\pi E_{beam}}{D} = \frac{\pi m_{beam} A_0^2 \omega^2}{D},$$

where m_{beam} is the mass of the beam.

2.3.2 Molecular Dynamics Review

Previous work on air damping in this regime focused on oscillating microbeams operated in low vacuum. Early work employed Christian's free molecular theory [6] in which the Maxwell-Boltzmann velocity distribution function is used for gases. It was found that the theoretical prediction of the quality factor is almost one order higher than the experimental results [37]. In an attempt to bring the theoretical values closer to the experimental measurements, Kadar introduced a modification to Christian's method that involved a new molecular speed distribution function (the Maxwellian-Stream distribution), reducing Christians quality factor results by a factor of π [16]. Li modified Kadar's Maxwellian- Stream (MS) distribution function to account for the velocity of the contact surface [18]. This further reduced Kadar's quality factor results, bringing the analytical solution even closer to the experimental results of Zook [37]. By pointing out the importance of the effects of damping caused by a nearby wall, Bao introduced the energy transfer model as a way of directly calculating the energy loss [1]. He has shown that his results are closer to the experimental results than those based on Christians model. In [1], Bao also claims that that, in the work of Kadar *et al*, the velocity distribution function is applied redundantly and therefore is theoretically incorrect, although no justification is given. With the relatively confusing literature, a careful examination of the previous models is necessary.

2.3.2.1 Christian's Free Molecular Model

Christian's free-molecular model was developed initially to model gas damping of a vane or fiber that is free to swing (like a pendulum) in a low vacuum [6]. Given such a vane or fiber, its behavior can be modeled as a spring-mass-damper system. Assuming that there is no friction at the hinge of the vane and that the angular displacement θ is small, the torque balance equation for this system will be

$$I\ddot{\theta} + G\dot{\theta} + m_v gr\theta = 0, \tag{10}$$

where, I is the moment of inertia of the vane about the pivot point, m_v is the mass of the vane, g is the gravitational acceleration, r is the distance from the center of mass to the

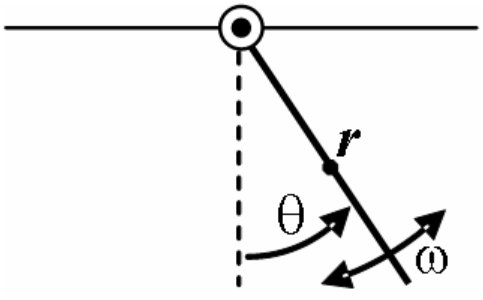

Figure 7: Schematic of a Vane Oscillating in Low Vacuum

pivot point, and G is the damping ratio. The solution to equation (10) is

$$\theta = \theta_0 e^{-at} \cos \omega t, \tag{11}$$

where, $a = G/2I$ and ω is the frequency of oscillation ($\omega = \sqrt{g/r}$, for $G \ll I$).

For an infinitesimal area dA of the vane at distance L from the hinge, the damping torque on this area will be $dG\dot{\theta} = dGu/L$, where u is the linear velocity of the area. The damping torque is also equivalent to $P_d dAL$, where P_d is the pressure difference between the front and back sides of the vane. Therefore, the damping coefficient can be expressed as

$$dG = \frac{P_d dAL^2}{u}. \tag{12}$$

The total damping ratio corresponding to the total damping torque will be

$$G = \frac{P_d}{u} \int L^2 dA = \frac{P_d}{u} J, \tag{13}$$

where J is the second moment of the projected area normal to the direction of motion. It is shown in the literature that the ratio P_d/u is independent of the vane dimensions.

The resistive damping force on the oscillating vane was found by determining the momentum transfer rate from the vibrating vane to the surrounding air due to the collisions between the vane and the molecules [6]. For one molecule striking the surface of the plate, the momentum change of the molecule will be $-2mv$, where m is the mass of the molecule and v is the molecule's velocity. For a plate lying in a plane normal to the x-direction moving in the x-direction with velocity u, molecules striking this plate will have a velocity $(v-u)$ at the back and $(v+u)$ at the front. Using Newton's second law, the pressure exerted on the vane is twice the rate of the change of momentum in the x-direction. Considering the velocities of the molecules relative to the plate, the force acting on the plate will be equivalent to the momentum transfer rate, or $F = dp/dt = (-2m(v \pm u))/\Delta t$, where p is the momentum. By summing up the resulting forces due to the impacting of the individual molecules on the vane, the pressure due to the molecule interactions can be found by dividing this total force by the area of the plate.

The number of individual molecules that will strike the surface are those contained in the "control volume" $V = v_r dt dA$, where v_r is the relative velocity of the molecule with respect to the surface and dA is the area of the surface, as shown in Figure 8. By using

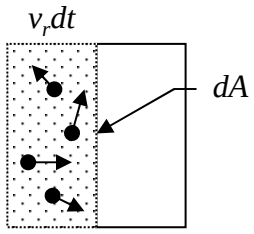

Figure 8: Control volume of molecules striking a surface within time dt having velocities in the range v and $v + dv$

the Maxwell-Boltzmann (MB) velocity distribution function, Christian showed that the

number of molecules striking the front and back surfaces of the vane per unit time per unit area are $(v+u)dn$ and $(v-u)dn$ respectively for those molecules whose velocities lie between v and $v+dv$, where

$$dn = nMB(v)dv = n\left(\frac{m}{2\pi kT}\right)^{\frac{1}{2}} \exp\left(-\frac{mv^2}{2kT}\right) dv.$$

Thus, the differential pressure on the vane becomes

$$P_d = n\left(\frac{2m^3}{\pi kT}\right)^{\frac{1}{2}} \int_0^\infty \exp\left(-\frac{mv^2}{2kT}\right) \left[(v+u)^2 - (v-u)^2\right] dv = 4\sqrt{\frac{2}{\pi}} uP\sqrt{\frac{m}{kT}}, \tag{14}$$

where n is the molecular density, m is the mass of one molecule, k is the Boltzmann constant and P and T are the pressure and temperature of air. Since $m = Mk/R_0$ and $n = P/kT$, where M is the molecular mass, k is Boltzmann's constant, R_0 is the universal gas constant, P is the gas pressure, and T is the absolute gas temperature, the differential pressure and resulting damping coefficient become

$$P_d = 4\sqrt{\frac{2}{\pi}} uP\sqrt{\frac{M}{R_0 T}} \tag{15}$$

$$G = 4\sqrt{\frac{2}{\pi}} P\sqrt{\frac{M}{R_0 T}} J. \tag{16}$$

The quality factor of the vane can then be calculated based on

$$Q = \frac{\omega\Theta_0}{G} = \left(\frac{\pi}{2}\right)^{\frac{3}{2}} \frac{f\rho_{Si}d}{P}\sqrt{\frac{R_0 T}{M}} \tag{17}$$

where ω is the oscillation frequency, Θ_0 is the moment of inertia of the vane, f is the oscillation frequency, ρ_{Si} is the density of the vane material (Silicon), and d is the thickness of the resonator.

The Free Molecular Model follows the widely accepted Kinetic Theory of Gases as described in Section 2.2.2. Christian's approach for calculating the quality factor is valid only if the vane is oscillating in an "unbounded" space, i.e., there are no nearby walls. For most MEMS applications, however, there is often a fixed wall (the substrate or electrodes, for example) near the oscillating structure. Thus, Christian's approach must be modified to account for the effects caused by the nearby wall. This is evident from the comparison between experimental measured quality factors of a oscillating microbeam and the theoretical predictions based on Christian's model as in [22, 37].

2.3.2.2 Kadar and Li's Modifications to the Free Molecular Model

Kadar

To bring theoretical predictions of the quality factor of the microbeam closer to the experimental results, Kadar *et al* sought to correct Christian's model based on the belief that the Maxwell-Boltzmann (MB) velocity distribution function used by Christian is inappropriate because it describes the velocity distribution of molecules in a gas as a whole, not the distribution function of molecules that actually collide with the beam [6]. Kadar modified Christian's theory by applying the Maxwellian-Stream (MS) distribution. The MS distribution function describes the velocity distribution of molecules based on a group of particles of an equilibrium gas that strike a surface. For a surface lying in the xy-plane, the MS is

$$MS(v_z) = \frac{m}{kT} v_z \exp\left(-\frac{mv_z^2}{2kT}\right) \tag{18}$$

By replacing the MB distribution with the MS distribution and following the exact same procedure as that used in implementing Christian's FMM, Kadar *et al*,using this modification, have reduced the calculated quality factor from Christian's results by a factor of π, bringing the theoretical value closer to Zook's data from his resonating microbeam experiment [37].

Li

In their paper, Li *et al* proposed that the MS velocity distribution used in Kadar's paper does not take into account the differences in the number and velocity distribution of molecules impacting on two sides of a vibrating microbeam [18]. Li showed that based on the relative velocities of molecules, the velocity distribution (MU) for molecules striking the front and back sides of the beam are

$$\begin{aligned} MU(v_z)_{front} &= \frac{m}{kT}(v_z + u)\exp\left(-\frac{mv_z^2}{2kT}\right) \text{ and} \\ MU(v_z)_{back} &= \frac{m}{kT}(v_z - u)\exp\left(-\frac{mv_z^2}{2kT}\right). \end{aligned} \tag{19}$$

The resulting quality factor reduced Kadar's result by another factor of 1.5, bringing the theoretical values even closer to Zook's experimental data. Figure 9[2] shows a comparison

[2]The $\mathbf{MB}(v_z)$ function represents the one-dimensional velocity distribution of the gas and includes the

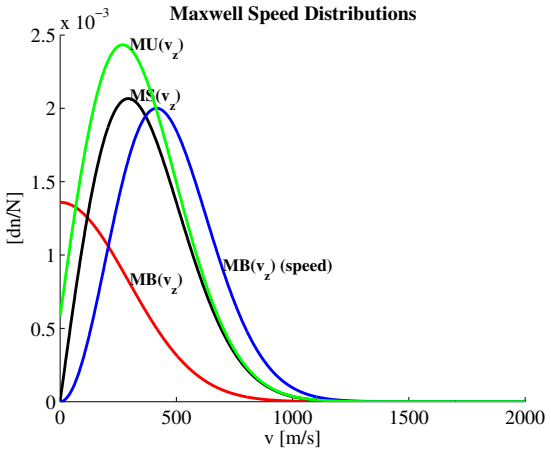

Figure 9: Gas Velocity Distribution Functions

of the forms of the three distribution functions for a gas temperature of 273 K.

2.3.2.3 Bao's Energy Transfer Model

In [1], Bao *et al* proposed a direct approach to determine the energy transfer between a resonating device and the equilibrium gas that surrounds it. This approach accounts for the effects of nearby walls as well as the dimensions of the oscillating device. By assuming elastic collisions between gas molecules and a resonating structure and ignoring the intermolecular collisions, Bao's model keeps track of the collisions of molecules with the moving structure and uses the conservation of linear momentum and conservation of kinetic energy laws to calculate the velocity change of a molecule after each collision. The total kinetic energy change of molecules is then found based on the initial and final velocities of the molecules.

To derive a formula (equation (17) in [1]) for energy dissipation of the resonating microbeam, Bao *et al* have made the following major assumptions:

- Constant Particle Velocity
- Constant Change in Particle Velocity

direction. The **MB(v_z)(speed)** function only represents the one-dimensional distribution for the magnitude of the gas molecules.

- Constant Beam Position

With these assumptions, Bao *et al* first calculated the number of collisions that each molecule will have with the beam. Based on this number, the change of energy of each molecule was computed. By summing up the changes of energy of all the molecules that will interact with the beam within one period of oscillation, the quality factor of the microbeam was then computed. It should be pointed out that in order to obtain an analytical expression of the quality factor of the microbeam, Bao *et al* used a molecule whose initial speed is the average speed of the gas as a "representative" molecule. The sum of the energy changes of all the molecules was obtained by multiplying the energy change of the representative molecule with the number of molecules interacting with the beam per unit time and integrating over the cycle of the beam. The resulting dissipated energy and quality factor are given in equation (20) and equation (21).

$$\Delta E_{cycle} = \frac{\pi \bar{l}^2 A_0^2 \omega}{16} \rho_0 \bar{v} \frac{L}{d_0} \tag{20}$$

$$Q_{Bao} = \frac{2\pi \frac{1}{2} M_p A_0^2 \omega^2}{\Delta E_{cycle}} \tag{21}$$

By applying this model to the oscillating microbeam, Bao *et al* have shown that the calculated quality factor compared more favorably with the measurements from Zook's microbeam experiment than the results from using Christian's model. This is largely due to the fact that in Bao's model, the effects of the nearby wall on the damping are considered.

2.4 Summary of Analytical Methods

Continuum theory applies when the rarefaction effects of the gas are negligible. The behavior of the gas in this regime is described by the Navier-Stokes equations for the flow of a fluid. To account for rarefaction effects, there are variations of the Navier-Stokes equations which use an effective viscosity, but they are only approximations of non-continuum behavior using continuum techniques.

The two molecular dynamics models discussed in this chapter become applicable when the gas rarefaction effects become significant. Because of this, these theories are valid only

for the free molecular regime. Using the rate of momentum transfer on a moving surface due to impinging gas molecules, Christian's free molecular model can be used to determine the damping force acting on the surface for a low vacuum environment [6]. Because it uses the distribution of gas molecules in equilibrium for an infinite space, its application is limited to cases that do not have nearby walls. Kadar's and Li's modifications to the free molecular model are based on changes to the gas velocity distribution function, and are still susceptible to the same limitations as the original model. Bao's energy transfer model takes into account the momentum and energy changes of the molecules colliding with the moving surface. It also attempts to account for the effects of nearby walls and makes the determination of the energy dissipation dependent on the geometry of the device.

CHAPTER III

ANALYSIS OF THE AIR DAMPING OF MICRORESONATORS

3.1 Introduction

To determine the quality factor of a microresonator, the energy transfer between the device and the gas surrounding it must be modeled accurately. In Section 2, two analytical methods for determining the damping of the device by air were given: Christian's Free Molecular Model (FMM) and Bao's Energy Transfer Model (ETM). While Christian's model does look at the interactions of individual molecules with the resonator surface, it does not account for the presence of a nearby wall. Most MEMS resonating devices are fabricated such that the gap between the resonator and the electrodes that drive them is on the order of microns or sub-microns. In this type of configuration, there will be squeeze-film damping effects, as well as a need for the time history of the molecules impacting the surface, as their past and present velocities (along with the device dimensions) will govern how much interaction each molecule has with the resonator and the other molecules in the gas. This chapter looks closely at the Free Molecular and Energy Transfer Models, and their limitations when applying them to popular resonator devices.

3.2 Analytical Study

3.2.1 Errors in Kadar's and Li's Modifications to the Free Molecular Model

The Free Molecular Model (FMM) developed by Christian is limited in its application to current MEMS technologies in that it does not account for the presence of a nearby electrode or substrate. As discussed in Section 2, Kadar improved the agreement between the theoretical results (using the FMM) and the experimental results given by Zook [37] by introducing a new gas velocity distribution function, the Maxwellian–Stream (MS) distribution. Bringing the theoretical results even closer to the experimental values, Li further

modified Kadar's MS distribution to account for molecules impinging on both sides of the resonator surface. Despite improvement in the agreement with experimental measurements, there are two fundamental mistakes in Kadar's approach.

The first mistake is in the calculation of the number of molecules striking the microbeam using the Maxwellian-Stream distribution function. In Christian's model, the number of molecules striking the microbeam within time dt is calculated by constructing a control volume of $V = v_r dA dt$, where v_r is the relative velocity between the gas molecule (v) and the beam (u), and dA is the striking area. Only those molecules which lie inside this volume will strike the beam within dt. Thus, the number of molecules that strike the beam within time dt and with area dA is $n \cdot \int_0^\infty V \cdot MB(v)dv$. In Kadar's model, the Maxwellian-Stream (MS) distribution is used instead. Unlike the MB function that gives the velocity distribution of all the molecules in a general gas assembly, the MS function is the velocity distribution function of the molecules that strike the surface. Thus, when using MS to calculate the density of molecules that strike the microbeam, the correct value for the number of molecules should be $n \cdot \int_0^\infty MS^*(v)dv$, not the $n \cdot \int_0^\infty V \cdot MS(v)dv$ used in Kadar's calculation, where MS^* is the modified Maxwellian-Stream distribution, as discussed in the next paragraph.

A second mistake comes from the coefficient in the MS distribution function. Directly adopted from [10], the coefficient in $C(c)$ used in Kadar's model is $\frac{1}{2}\left(\frac{m}{kT}\right)^2$ ([16], equation (12)). This coefficient, however, is obtained by considering only the molecules that strike the surface, i.e., integrating this distribution function in the velocity space gives only the total number of molecules that strike the surface, not the total number of gas molecules as a whole. The correct approach should be either changing the coefficient to $\frac{m}{2kT}\sqrt{\frac{m}{2\pi kT}}$ or using the coefficient of $\frac{1}{2}\left(\frac{m}{kT}\right)^2$, but changing n to be the molecular density of those striking the wall. With the correct way of computing the density of molecules that strike the beam using the MS distribution function, the net pressure acting on the microbeam is

$$P_d = 2m \int_0^\infty \left[n \cdot \sqrt{\frac{m}{2\pi kT}} \exp\left(-\frac{mv^2}{2kT}\right)(v+u)^2 - n \cdot \sqrt{\frac{m}{2\pi kT}} \exp\left(-\frac{mv^2}{2kT}\right)(v-u)^2 \right] dv. \tag{22}$$

In equation (22), n is the molecular density of the gas as a whole. Taking the common factors out of the integral, the above equation corresponds exactly with the pressure equation derived from Christian's model equation (14). This is not surprising since the fundamental principle used in Christian's and Kadar/Li's approaches is the same. The Maxwellian-Stream distribution function can be derived from the Maxwell-Boltzmann distribution function and the "control-volume" approach used by Christian.

3.2.2 Bao's Energy Transfer Model

Bao's Energy Transfer Model (ETM) provides a closer approximation of the experimental results, while taking into account the resonator's geometry and the presence of nearby walls. A close examination of Bao *et al*'s results revealed that a better fit seems to be around the pressure range of 10 torr which is corresponding to a Kn number of 4.5. In this range, gas is in the transition regime and intermolecular collisions are important. Based on the assumption of free molecular flow (i.e., ignoring the intermolecular collisions), it seems that Bao's model should fit better at pressures lower than 5 torr. This fact calls for a careful examination of Bao's major assumptions.

3.2.2.1 Bao's Major Assumptions

There are three major assumptions made in the development of the ETM. These were listed in Section 2.3.2.3 and are described below in detail. They are as follows:

1. **Constant Particle Velocity** - In the calculation of the number of collisions of one particle with the beam for the entire period of interaction with the beam, the velocity of the particle is assumed to be fixed and is equal to its initial value.

2. **Constant Change in Particle Velocity** - The time for a gas particle staying under the microbeam (travel time) is much smaller than the oscillating cycle of the beam. Therefore, the velocity gained or lost by a particle after each collision remains the same during its travel time.

3. **Constant Beam Position** - The amplitude of oscillation of the beam is much smaller than the gap between the beam and the nearby stationary wall (substrate in the

microbeam case). Therefore, the gap is assumed to be constant during the travel of the molecule.

The "constant velocity" assumption applied in Bao's model allows for a much simpler analytical expression for the number of collisions ΔN, given by equation (23)

$$\Delta N = \frac{l v_{x0}}{2\,(d_0 - x)\,v_{yz0}} \tag{23}$$

where l is the distance the molecule travels in the gap, d_0 is the initial gap between the beam and the stationary wall, x is the displacement of the beam as it oscillates (which is assumed to be constant due to the third assumption), and v_{x0} and v_{yz0} are the initial velocities of the molecule in the x- and yz-directions, respectively. This formula implies that the number of collisions of a gas molecule whose velocity increases each time when it collides with the beam is the same as that of a molecule whose velocity decreases each time when it collides with the beam. Such an assumption, however, could underestimate the energy gained by the gas molecules because the number of collisions of molecules that gain velocity at each collision is larger than the number of collisions of molecules that lose velocity. To illustrate this, the path of a molecule (as a function of time) is shown in Figure 10. Figure 10(a)

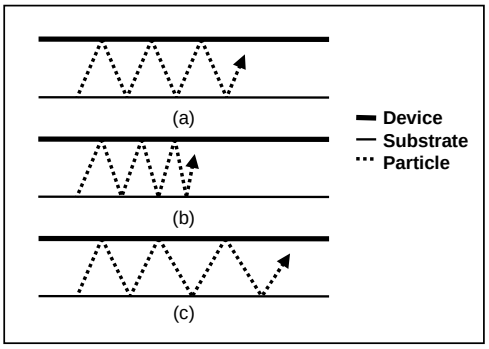

Figure 10: The Effects of the "Constant Velocity" Assumption

corresponds to the case in which the velocity of a gas molecule remains constant during the interaction. Figure 10(b) shows the case where the beam's motion is downward and the vertical velocity of the molecule increases after each collision, resulting in an increase in the number of collisions for the same interaction time. Similarly, Figure 10(c) represents the

case in which the vertical velocity of the molecule decreases each time it collides with the beam as the beam moves upward. As illustrated in the figure, if the velocity of the molecule increases or decreases after each collision, the time between two consecutive collisions will decrease or increase. For the same travel time (determined by l and v_{yz0}), the number of collisions will then be different. With the "constant velocity" assumption, the number of collisions of molecules that gain velocity is underestimated while the number of collisions of molecules that lose velocity is overestimated. Since the final velocity of the molecule (kinetic energy) is based on the number of collisions, this assumption results in an over-predicted value of the quality factor. As shown in Section 4.2.4, such an overestimation is quite significant.

The second assumption is that the time for a gas molecule staying under the microbeam (travel time) is much smaller than the oscillating cycle of the beam. Therefore, the velocity of the beam during its interaction with a molecule is regarded as a constant. This implies that the velocity change of a molecule after each collision remains the same during its travel time. Such an assumption is reasonable for the microbeam being studied, as the travel time of a molecule under the beam is almost one order smaller than the oscillating period of the beam. This assumption also allows for the determination of the dissipated energy without taking into account particles that would remain under the microbeam when the oscillating period is on the same order or smaller than the travel time.

The third major assumption is that the amplitude of the oscillating device is much smaller than the gap between the moving device and any nearby walls. By this assumption, the device can be seen as stationary (distance-wise), thus further simplifying the calculation for the number of collisions that each molecule will have with the device. For the microbeam case, this assumption follows logically from the geometry and actuation mechanisms of the device.

Although the second and the third assumptions are reasonable for the microbeam case, they may pose a limitation on the scope of applications of Bao's model to a more general class of resonant devices.

3.2.3 Review of the Limitations of the Analytical Methods

3.2.3.1 Christian's Free Molecular Model

Christian's free molecular model is limited in application to low pressure cases in which the gas is rarefied and there are almost no interactions between gas molecules. At higher pressures, where these intermolecular collisions will occur, the history of each particle that collided with the moving surface would have to be known. This is because these molecules will collide with other nearby molecules, changing their velocities and effecting the entire velocity distribution of the gas molecules in the interaction region. It is also possible for a molecule to collide with the surface again after colliding with another molecule.

Not knowing the history of the molecules also leads to the other limitation of Christian's model, which hinders its effective use in the analysis of MEMS devices. The free molecular model does not account for the presence of nearby surfaces that could cause the molecules to return to the device surface for subsequent collisions. This effect becomes significant as the same molecules collide with the device several times, and then leave the interaction region with a possibly greater net increase in kinetic energy. This would mean that the energy that leaves the system with the gas molecule was lost by the device, increasing the estimated amount of energy dissipation of the device and decreasing the calculated quality factor.

3.2.3.2 Bao's Energy Transfer Model

The limitations of Bao's energy transfer model stem from its major assumptions. The "constant velocity" assumptions results in an underestimation of the energy dissipation because the velocity of the beam is time-dependent and the subsequent change in velocity of the particles will vary with the time of collision. Also, when the velocity of the particles is updated after every collision, the increase and decrease in the total number of collisions between the particle and the beam due to the varying beam velocity can be captured (see Section 3.2.2 for more details).

The second assumption limits the energy transfer model only to cases where the operating frequency of the beam is much larger than the particle travel time. The energy transfer

model cannot be used in cases where the travel time is less than the period of oscillation because it has no way of accounting for the effects of particles trapped under the beam after the oscillation period.

The third assumption also has an effect on the number of collisions between the particle and beam. This condition limits the application of the energy transfer model because as the amplitude increases, the number of collisions will increase as the the beam moves toward the other wall, resulting in a greater energy gain, and will decrease as the beam moves away from the other wall, resulting in a smaller energy loss of the particle.

CHAPTER IV

NUMERICAL STUDY OF THE SQUEEZE-FILM DAMPING OF MICRORESONATORS

4.1 Introduction

As discussed in the previous chapter, the continuum and free molecular analytical methods have limitations when it comes to device geometry and non-continuum effects. These limitations on the analytical approaches led to the investigation of numerical simulation techniques to bring the theoretical results closer to results from existing experiments. A molecular dynamics simulation was developed in order to verify the energy transfer model and provide a better estimation of the energy dissipation. The simulation was also used to determine the effects of the pressure, beam oscillation frequency, and beam oscillation amplitude on the energy dissipation. In this chapter, a detailed description of the molecular dynamics simulation is given. The results from the analysis of the microbeam resonator using the simulation are presented and discussed.

4.2 Molecular Dynamics Simulation Method

4.2.1 Development

4.2.1.1 Simulation Description

The molecular dynamics (MD) simulation is a useful tool for estimating the damping of resonators in a very rarefied gas environment. Because of the very low number of intermolecular collisions in a rarefied gas, it becomes possible to track the motion of each molecule. There are four main characteristics of the general MD simulation. These are the simulation domain, the representative particle, the discretization of the moving surface's period of oscillation, and the calculation of the quality factor.

Simulation Domain

The simulation domain consists of two solid walls that are parallel to one another.

One of these walls is fixed while the other experiences a time-dependent sinusoidal motion $x_w(t) = A_0 \sin(\omega t + \tau)$. The moving wall has an oscillation frequency f. The initial velocity (or phase) of the wall is based on the current division of the device's oscillation period and is given as $u(t) = A_0 \omega \cos(\omega t + \tau)$, where A_0 is the amplitude of the device's oscillation as set by the Gap/Amplitude ratio, $\omega = 2\pi f$, t is the current simulation time (which starts at 0 for all period divisions), and τ is the simulation division offset as determined by the number of period divisions *perdiv* ($\tau = k \cdot (1/f)/perdiv$, where k is one less than the value of the current period division). Figure 11 shows a schematic of the simulation domain for a microbeam resonator. To reduce simulation time, the y- and z-dimensions were combined

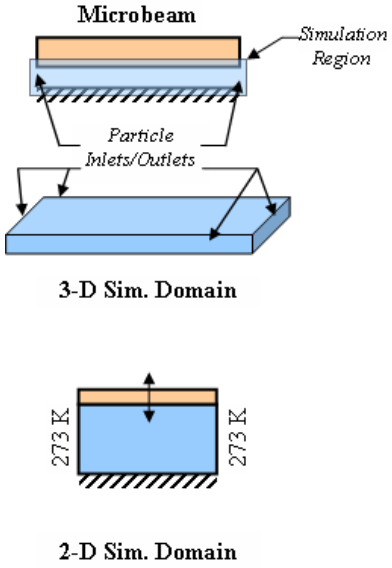

Figure 11: Simulation Domain for the Microbeam Case

as the average travel distance ℓ of the particle (Figure 12). The average travel distance for the simulation particle is approximated by the relation $\ell = \sqrt{2ab/\pi}$ [1].

Simulation Particle

Because the molecular dynamics simulation is based on a free molecular dynamics model, it only accounts for the interactions of individual molecules with a moving surface. One particle of a gas with an initial velocity $\vec{v}_i$ and initial position is chosen as a representative particle of the equilibrium gas surrounding a resonating device. Each component of its initial velocity is chosen according to the three-dimensional Maxwell-Boltzmann (MB) gas

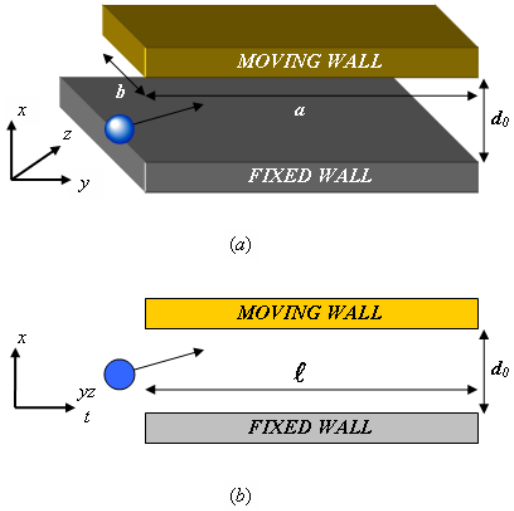

Figure 12: Simplification of the Simulation Domain

velocity distribution function. Because the one particle is used to represent all of the molecules interacting with the device during a set period of time, its initial velocity is set to the average velocity of this distribution ($\vec{v}_i = \sqrt{8RT/\pi M}$, where $\vec{v}_i = \sqrt{v_{xi}^2 + v_{yi}^2 + v_{zi}^2}$). The y- and z-directions form a plane that is parallel to the device's moving surface and the fixed wall. The x-direction is the gap dimension, which is normal to the yz-plane. As the particle enters the gap between the device and the substrate (or electrode), its position and velocity are tracked. When the particle is set into motion, its position is calculated by multiplying the simulation time step by the particle's x-velocity and adding this displacement change to its previous position ($x_2 = x_1 + v_{x1}\Delta t_{MD}$, where Δt_{MD} is the simulation time step). The period of time that the particle is allowed to interact with the device is calculated based on the y- and z- components of the particle velocity. This value is calculated by dividing the average travel distance ℓ (which is calculated based on the dimensions of the device) by the velocity of the particle in the yz-plane (v_{yzi}). This ratio is a constant value since the particle's velocity in the yz-plane is assumed to remain constant throughout its interaction with the device. For each simulation step, the particle's velocity and position are updated. The position of the particle is then compared with the position of both walls. If the particle "passes" either wall, its velocity is reversed, marking

a collision with a solid surface. Collisions between the particle and the walls are assumed to be purely elastic. When it contacts the moving wall, the magnitude of the particle's velocity is incremented according to the wall's current velocity: $v_{x2} = v_{x1} + 2u(t)$. The derivation of this velocity increment is given in Section 2.2.2. The particle's position and velocity are continually updated in this fashion until the average travel distance is reached. The change in kinetic energy of the particle is calculated as $\Delta E = \frac{1}{2}m\left(v_{xf}^2 - v_{xi}^2\right)$, and the result is scaled based on the number of molecules Δn that will enter the simulation region (gap between the device and electrode) within a set time.

Simulation Period Division

The time used to calculate the number of particles entering the simulation region is actually the size of the discretization of the oscillation cycle of the moving wall. These discretizations are referred to as period divisions. This input can be varied by the user, and the accuracy of the simulation increases as the number of period divisions increases. The period division is necessary because the phase of the device oscillation is changing, thus particles entering the region at different times will experience different interactions with the device. The period division is used to set the time offset of each simulated particle, which is then used to set the current simulation time. The particle's motion starts at this time and ends when it has traveled the average travel distance in the yz-plane. The number of molecules entering the gap per period division is given as $\Delta n = \frac{1}{4}n\bar{v}Lx_w\Delta t$, where L is the peripheral length of the device ($2a + 2b$ for the beam), n is the number density of the gas molecules, x_w is the position of the moving wall (i.e., the actual gap size), $\bar{v}$ is the average velocity of the gas molecules according to the *MB* distribution, and Δt is the length of the period division [6]. The simulation time step Δt_{MD} was chosen to be $perdiv/50000$, resulting in a very small displacement of the particle per time step.

Quality Factor

To obtain the quality factor of the microbeam, the energy dissipation for an entire oscillation cycle is needed. To obtain this, the oscillation cycle is divided into several divisions (period divisions) and the change in kinetic energy of the simulation particle due to its interaction with the moving surface is calculated for each period division. The total

energy transferred between the device and the particle for an entire oscillation cycle is found by taking the sum of the energy changes from each period division. The result is then scaled based on the number of particles Δn interacting with the device per period division. Thus, the total energy transferred between the moving wall and the simulation particle will be

$$\Delta E_{cycle} = \Delta n \sum_{i=0}^{perdiv} \Delta E_i = \Delta n \sum_{i=0}^{perdiv} \frac{1}{2} m \left[\left(v_{xf}^2 - v_{xi}^2 \right) \right]_i .$$

4.2.1.2 Simulation Variations

There are four main variations of the molecular dynamics simulation. Each variation addresses a particular simulation issue. The first variation is discussed in the previous section and represents the general case using one simulation particle. The second variation was developed to duplicate Bao's energy transfer model (ETM) numerically. It follows the same rules as the general case, but with a few exceptions. In this variation, each particle begins from the same position in the $x-$direction. If the particle strikes the moving wall, the particle's velocity is reversed and it's magnitude is unchanged. The change in velocity that the particle would have experienced is stored. A running sum of these velocity changes is kept throughout the travel time of the particle. A counter also keeps track of the number of collisions that the particle has with the device. At the end of the particle's travel time, the sum of the changes in velocities is added to the magnitude of the particle's initial velocity, giving its final velocity. The total energy change and resulting quality factor are calculated in the same manner as in the general case. Figure 4.2.1.2 shows the trajectory of the simulation molecule for one period division. The solid black line represents the nominal beam position, while the blue line shows the actual beam position. As with Bao's energy transfer model, the position of the beam is held constant.

For the third variation of the MD simulation, the major assumptions used in Bao's ETM were relaxed. The particle velocity was updated after each collision with the beam and the beam's position and velocity were time-dependent. The energy dissipation and quality factor are still determined in the same manner as in the first variation. The results from these first two variations were compared and are described in detail in Section 4.2.4.2. Figure 4.2.1.2 shows the process flow for this variation.

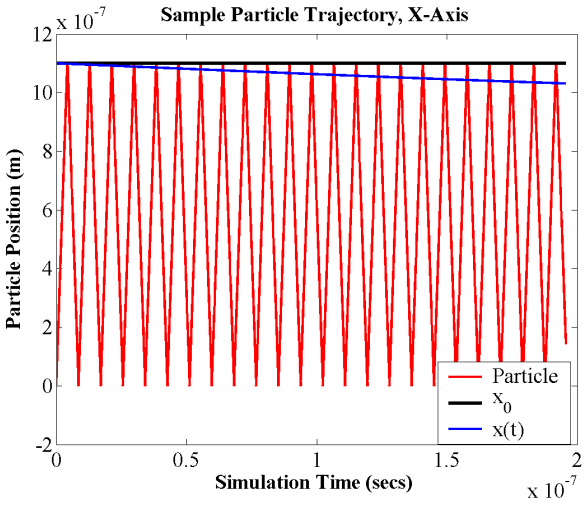

Figure 13: Sample Trajectory of an MD Simulation Particle for Bao's ETM Variation

The fourth variation was developed in order to test the validity of choosing one simulation particle with the average characteristics of the gas. To do this, several particles were simulated with varying initial velocities and positions. The initial positions of these particles were assigned according to a uniform random distribution. The velocities were assigned according to the Maxwell-Boltzmann velocity distribution, as shown in equation (24)

$$v_{xi} = \sqrt{\frac{2k_B T}{m}}\,\text{erfinv}(2y_i - 1), \tag{24}$$

where erfinv is the inverse error function, and y_i is a uniformly distributed random number from -1 to 1. The development of this relation is discussed in greater detail in Appendix C. At each period division, N particles are simulated and the resulting kinetic energy changes are averaged and stored. These stored values are then added to the energies from all of the other period divisions, and the resulting energy dissipation for the cycle is obtained.

4.2.2 Strategy and Implementation

Because of its flexibility and simplicity, the Molecular Dynamics (MD) simulation can be used to estimate several cases for the damping of a resonating microbeam. For instance, the code can be modified such that the effect of each of Bao's assumptions can be studied, as in the third variation discussed in the previous section. For example,

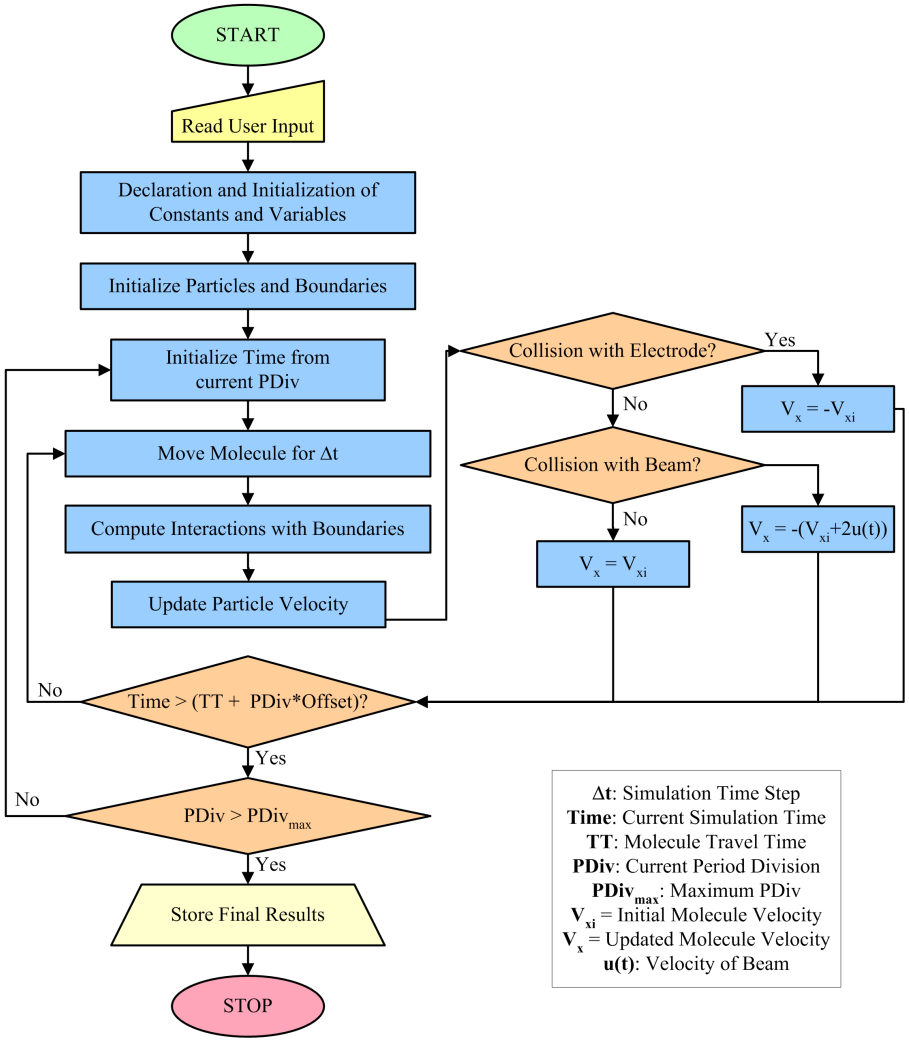

Figure 14: Process Flow of the MD simulation

- The microbeam's displacement can be held constant or allowed to change with time;
- The velocity of the particle can remain constant during the interaction and the resulting velocity change added afterward;
- The particle velocity can be changed with each interaction with the microbeam; or
- The initial position of the molecule can also be modified.

Using the average travel distance of the particle, given as $\bar{l} = \sqrt{2ab/\pi}$ (where a is the length of the beam and b is the width), along with the average velocity according the the MB gas velocity distribution$\left(\bar{v} = \sqrt{8kT/\pi m}\right)$, the average travel time per particle is $\bar{l}/\bar{v}$.

The input parameters for the program are the number of period divisions, the operating frequency in Hz, the gap to amplitude ratio (typically 10), the pressure in Pa, and the starting position of the molecule x_0 as a fraction C of the gap (Cd_0). Also, as discussed in Section 4.2.1.2, the simulation can be modified to handle multiple particles per period division N, where the initial velocity of these particles is selected randomly using the Maxwell-Boltzmann velocity distribution function. The geometry of the beam is known, and remains constant for each simulation, although the simulation can be easily modified to accommodate any rectangular geometry. The microbeam has dimensions $200 \times 40 \times 1.8$ micrometers with a 1.1 micrometer gap between the device and its driving electrode. Assuming that the gap d between the device and electrode is much larger than the amplitude A_0 of the device's oscillation ($d_0 \gg A_0$ or $10A_0 \leq d_0$), the amplitude of oscillation is estimated as $A_0 = d_0/10$. The driving/operating frequency of the device is 550 kHz. The resonator is assumed to be made out of silicon, with a density of 2330 kg/m^3. The oscillation period of the microbeam is 1/550K, which is 1.818×10^{-6} sec.

4.2.3 Limitations of the MD Simulation

In the development of the molecular dynamics simulation, there were several limitations that became evident. One primary limitation of the simulation is that it is only valid for the free molecular regime. The simulation does not account for interactions between molecules. Another limitation of the code is that it is only valid for operating frequencies with periods shorter than the average travel time of the particles. This is because the code assumes that, on average, the molecules that enter the region will leave the region before the oscillation period has ended. Without this assumption, there is no way to account for the molecules remaining under the beam at the completion of the period. Another limitation of the molecular dynamics code is that its use is restricted to rectangular domains, with four particle inlet/outlet boundaries. For example, the code would be unable to simulate the squeeze-film effects on a laterally-oscillating disk, which has two inlet/outlet boundaries, because it cannot account for particles that will remain in the simulation region for several oscillation periods.

4.2.4 Applications of the Molecular Dynamics Simulation

4.2.4.1 Simulation Parameters

Figure 15 shows the schematic of a microbeam resonator. The microbeam is modeled as a rigid body, thus it can be treated as two parallel plates for simulation purposes. The top plate represents the microbeam which is oscillating at a frequency of 550 kHz. The amplitude of oscillation A_0 is set to be $\frac{1}{10}$ of the gap d_0, such that $A_0 \ll d_0$. The bottom plate represents the fixed substrate. The dimensions of the plates are 200 μm long, 40 μm wide, and 1.8 μm thick (top plate). The gap between the plates is 1.1 μm. All the parameters used in our calculations are consistent with those used in Zook's experiments so that a comparison can be made.

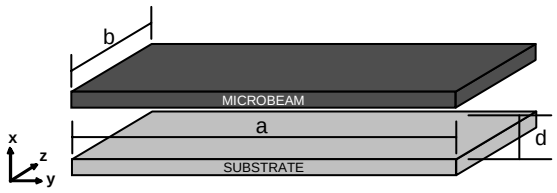

Figure 15: Microbeam Resonator Schematic

4.2.4.2 Study of the Effects of Bao's Assumptions

To examine the assumptions used in Bao's model, as listed in Section 2.3.2.3, the MD code was modified to calculate the quality factor of the microbeam with these assumptions removed. The lower curve in Figure 16 ($Q_{Sim,PV}$) shows the resulting Q-values when the molecular velocity is updated after each collision (i.e., no "constant velocity" assumption). It can be seen that the value converges to a little less than half of Bao's theoretical value. It is from this drop in quality factor that we can say that the "constant velocity" assumption is a significant source of error in the analytical solution. This phenomenon is described in detail in Section 2.3.2.3. As the other two assumptions are relaxed, as expected, the simulated quality factor changes slightly, bringing the total value of the Q-factor from 0.64528 to 0.75160. These results are represented by the curve $Q_{Sim,NA}$ in Figure 16. Table 3 shows a comparison of the simulated values with those from the analytical solution

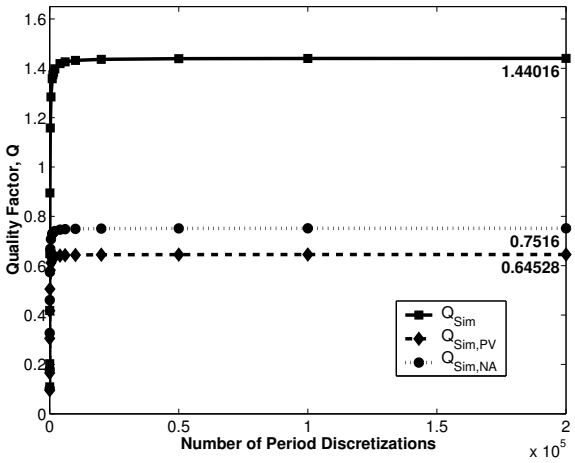

Figure 16: Simulation Results for Relaxed Assumptions

with increasing number of period divisions. As the number of period divisions increases, the simulated result continues to approach the analytical solution, converging to within 1% of the analytical value (see Table 3).

The third variation of the code was also used to simulate this case. This variation was found to be limited by the relatively small number of actual particles that could be simulated. For over 2 million total simulation particles, the simulation results did not converge to a reasonable value. It is believed that this was due to the statistical error that was inherent in the results, because of the size of the particle sample relative to the actual particle population. This was apparent even with weighting the results using the initial velocities of the particles and the the Maxwell-Boltzmann velocity distribution. The computational costs of simulating more particles outweighed the feasibility of using this variation, especially since the other variations were giving favorable results.

4.2.4.3 Comparison of Simulation results with Experimental and Theoretical Results

The goal of our simulations is to predict the energy dissipation, and thus the quality factor, of the microbeam when it resonates at its fundamental frequency (550 kHz) at standard temperature and at different ambient pressures. This is done by determining the damping due to a thin-film gas between the microbeam and its electrodes. Particular interest was

Table 3: Convergence of MD Simulation Results

$PerDiv$	Q_{Bao}	Q_{Sim}	$\%\ error$	$Q_{Sim,PV}$	$Q_{Sim,NA}$
5	1.4484	0.1091	92.4657%	0.0955	0.1022
10	1.4484	0.2029	85.9925%	0.1652	0.1790
25	1.4484	0.4188	71.0889%	0.3056	0.3274
50	1.4484	0.6489	55.2005%	0.4173	0.4605
100	1.4484	0.8948	38.2262%	0.5057	0.5741
250	1.4484	1.1580	20.0508%	0.5820	0.6683
500	1.4484	1.2839	11.3571%	0.6119	0.7075
1000	1.4484	1.3578	6.2606%	0.6280	0.7298
1250	1.4484	1.3736	5.1701%	0.6313	0.7327
1500	1.4484	1.3843	4.4289%	0.6335	0.7367
2000	1.4484	1.3980	3.4860%	0.6364	0.7403
4000	1.4484	1.4190	2.0362%	0.6409	0.7462
6000	1.4484	1.4261	1.5432%	0.6424	0.7480
10000	1.4484	1.4319	1.1452%	0.6436	0.7493
20000	1.4484	1.4362	0.8446%	0.6445	0.7506
50000	1.4484	1.4388	0.6633%	0.6450	0.7513
100000	1.4484	1.4397	0.6028%	0.6452	0.7515
200000	1.4484	1.4402	0.5725%	0.6453	0.7516

focused on the low pressure range as the MD simulation and the free molecular and energy transfer models are based on the assumption of free-molecule flow. For the microbeam resonator case, the free molecular regime at standard temperature (i.e., Kn $>$ 10) corresponds to a pressure range of $\approx$ 4.49 torr and under.

Figure 17 shows the simulated quality factors as functions of pressure (a) and Knudsen number (b). Also shown in the same figure are Zook's experimental and Christian's and Bao's theoretical results. Although based on the free-molecule assumption, Bao's results, represented by Q_{Bao}, most closely approximate the experimental values in the transition regime. The results from the simulation where the major assumptions were relaxed, as shown by curve $Q_{Sim,NA}$ of Figure 17, show that the calculated values agree well with the experimental values in the pressure range of 0.08 and 3 torr (i.e., the Knudsen number is between 561 and 15) which is consistent with the assumption of the free-molecule regime used in this study. Table 4 lists detailed values within this range. When the pressure is lower than 0.08 torr, the experimental curve flattens out and eventually approaches to a

constant value. This is due to the fact that at very low pressures, other loss mechanisms

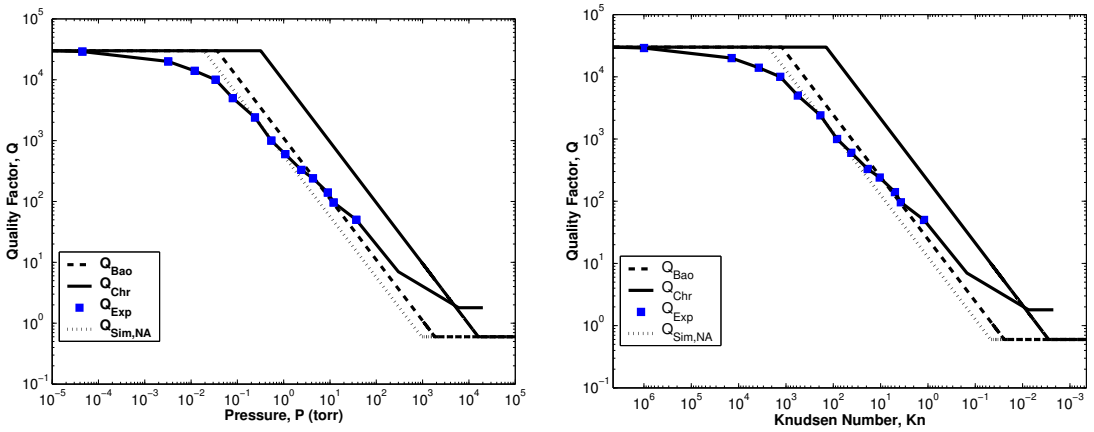

(a) Pressure vs. Quality Factor (b) Knudsen Number vs. Quality Factor

Figure 17: Quality Factor Results

Table 4: Simulated vs. Experimental Results.

P (torr)	Knudsen Number	Q, Simulation	Q, Experiment	% Error
0.034	1320.9224	16724.2375	10000	67.24
0.08	561.392	7107.8009	5000	42.16
0.24	187.1307	2369.267	2400	1.28
0.54	83.1692	1053.0075	1000	5.30
1.08	41.5846	526.5038	600	12.25
2.4	18.7131	236.9267	330	28.20
4.3	10.4445	132.2382	240	44.90

such as anchor loss and internal friction loss, which are independent of pressure, become significant as compared to the air damping and eventually dominate the energy loss. This explains the large discrepancy observed between the experimental data which includes all the loss mechanisms and the simulation results which only account for air damping at very small pressures. To estimate the experimental results due to air damping alone, it was assumed that at $P = 1 \times 10^{-6}$ torr, the damping is due only to the other loss mechanisms. The Q at this pressure is approximately $30,000$. Using this value of the quality factor to calculate the energy dissipation due to the other loss mechanisms, the energy dissipation due to the air damping was approximated. These results are given in Table 5 and shown in Figure 18. The approximated quality factors for the experimental air damping show that

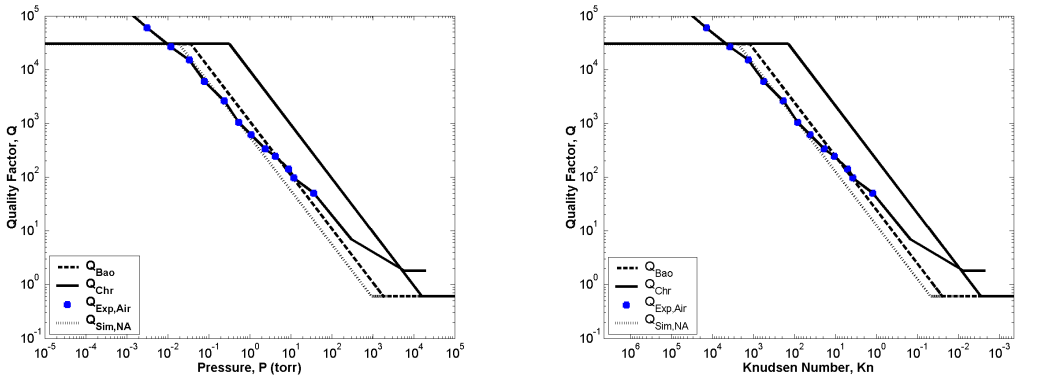

(a) Pressure vs. Quality Factor (b) Knudsen Number vs. Quality Factor

Figure 18: Adjusted Quality Factor Results

Table 5: Simulated vs. Adjusted Experimental Results.

P (torr)	Q, Simulation	Q, Exp. (Air)	% Error
0.034	16724.2	15000	11.49
0.08	7107.8	6000	18.46
0.24	2369.3	2608.7	9.19
0.54	1053	1034.5	1.79
1.08	526.5	612.2	14.01
2.4	236.9	333.7	29
4.3	132.2	241.9	45.44

the results from the MD simulation have better agreement in the free molecular regime than those from Bao's energy transfer model.

4.2.4.4 Effects of Oscillation Frequency and Amplitude on the Damping

When studying the gas rarefaction effects on the energy dissipation of microresonators, the important parameters that need to be analyzed are the gap between the beam and the substrate, the mean free path of the gas molecules, and the oscillation frequency and amplitude of the beam. The effects of these parameters can be characterized using three non-dimensional parameters: the Knudsen number, the Stokes number β equation (25), where ν is the kinematic viscosity, and the ratio of the gap to the oscillation amplitude d_0/A_0. The Knudsen number is a measurement of the degree of rarefaction and these effects have been discussed in the previous section. The Stokes number describes the effect

of the fluid drag on particle motion. In this section, the effects of the Stokes number and gap-to-amplitude ratio are studied, showing the effects of the oscillation frequency and amplitude on the damping.

$$\beta = \sqrt{\frac{\omega d_0^2}{\nu}} p \tag{25}$$

By varying the oscillation frequency while maintaining constant Knudsen number and gap-to-amplitude ratio, the dissipated energy D and the corresponding Q values at different Stokes numbers were simulated. Table 6 gives results corresponding to three different Stokes numbers. As indicated in the table, both damping and quality factor increase with

Table 6: Stokes Number dependence of the Dissipated Energy and the Quality Factor for a Knudsen Number $Kn = 100$ and $d_0/A_0 = 10$

Stokes Number, β	Dissipated Energy, D	Quality Factor, Q
0.01	3.24790E-18	4.23897E-01
0.1	3.96044E-16	3.47757E+01
1	2.65381E-14	5.18214E+03

increasing Stokes number. The main reason for the increase in damping is that as the frequency increases, the velocity gained by the molecules at each collision increases and thus the energy gained by the molecules increases as well. For the quality factor, the total energy pumped into the system is proportional to the square of the frequency. Thus despite an increase in damping, the quality factor increases with the frequency. In fact, when the frequency is small, it can be proven from Bao's formula that both damping equation (26) and quality factor equation (27) linearly depend on frequency.

$$\Delta E_{cycle} = \frac{\pi \bar{l}^2 A_0^2 \omega}{16} \rho_0 \bar{v} \frac{L}{d_0} \tag{26}$$

$$Q_{Bao} = (2\pi)^{\frac{3}{2}} \rho H \omega \left(\frac{d_0}{L}\right) \sqrt{\frac{RT}{M_m}} \frac{1}{P} \tag{27}$$

Similarly, the effects of the oscillation amplitude on the damping were studied by calculating the damping at different Strouhal numbers. Plots of the dissipated energy and the corresponding Q value versus the Strouhal number at constant Stokes and Knudsen numbers are shown in Figure 19. As expected, more energy is dissipated when the Strouhal number

is small (i.e., the oscillation amplitude is large). The large amplitude means that there are more collisions between gas molecules and the beam when the beam moves down (in which gas molecules gain energy) and less collisions when the beam moves up (in which gas molecules lose energy). The quality factor has a strong dependence on the gap-to-amplitude

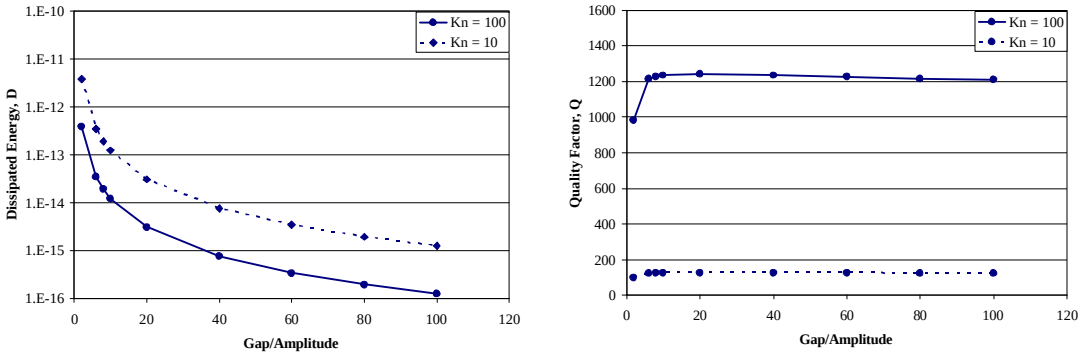

(a) Gap/Amplitude vs. Damping Energy (b) Gap/Amplitude vs. Quality Factor

Figure 19: Dependence of the Dissipated Energy and Quality Factor on the Gap-to-Amplitude ratio for an operating frequency of 550 kHz

ratio when it is small. It is, however, almost independent of the gap-to-amplitude when it is large. This fact is consistent with the theoretical prediction from Bao's formula in the small-amplitude cases.

CHAPTER V

SLIDE FILM DAMPING ANALYSIS OF A DISK RESONATOR

5.1 Introduction

In the case of laterally oscillating devices, viscous drag is the dominant damping mechanism. Previous studies have focused on devices moving as rigid bodies and at low frequency. For these cases, the incompressible flow assumption is used and is justified. When the device moves non-uniformly, compressibility effects could become important and need to be investigated.

For this study, the compressibility effects of a thin, fluid film between a laterally resonating, disc-shaped component and a fixed substrate is investigated. The disc performs radial oscillations that are induced by sinusoidal voltages across its diameter. An analytical solution to the pressure distribution is obtained, after which, the velocity distributions are derived. Since the ambient fluid is air and the gap is on the order of 1 micron, the well-known gas film theory equations are used together with the continuity equation for mathematical derivations.

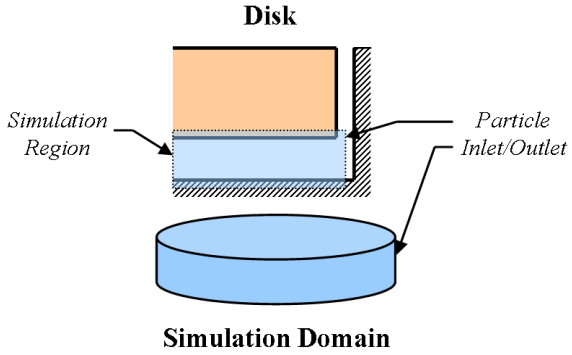

Figure 20: Disk-Shaped Resonator Schematic

5.2 Mathematical Formulation

The analysis begins with the gas film equations in the form of the Navier-Stokes momentum equation, given as

$$\frac{\partial\left(\rho\vec{V}\right)}{\partial t}+\nabla\bullet\left(\rho\vec{V}\vec{V}\right)=-\nabla P+\nabla\bullet\tau+\rho\vec{b}, \tag{28}$$

where ρ, $\vec{V}$, p, τ, and $\vec{b}$ are the air field density, velocity, pressure, viscous shear stress, and body force (which is most commonly characterized by the gravitational force acting on the fluid), respectively [23]. Since the fluid in question is contained in a nano-scale enclosure, Newtonian fluid effects are assumed to be prevalent and with the ensuing continuity equation,

$$\frac{\partial\rho}{\partial t}+\nabla\bullet\left(\rho\vec{V}\right)=0 \tag{29}$$

the Navier-Stokes equation reduces to the form

$$\rho\frac{d\vec{V}}{dt}+\rho\vec{V}\left(\nabla\vec{V}\right)=-\nabla P+\mu\nabla^2\vec{V}+\frac{\mu}{3}\nabla\left(\nabla\bullet\vec{V}\right)+\rho\vec{b}, \tag{30}$$

where μ is the fluid viscosity. The figure below presents a diagram of the current geometry, with the fluid film being constrained between two circular discs. One disk is assumed to be oscillating laterally while the other is fixed. The space between the two discs, or the

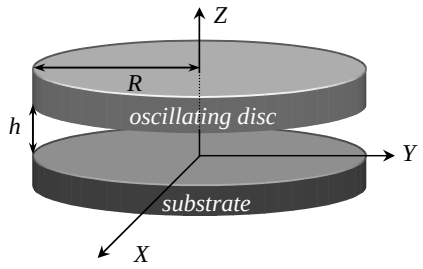

Figure 21: Geometry of Micro Resonator

height of the constrained air column, h, is much smaller that the radial dimension, R. For this resonator, the aspect ratio, R/h, is estimated to be on the order of 10. The fixed disk simulates the holding substrate while the oscillating disk oscillates at a frequency, ω,

in the vicinity of 10^9-hertz and for the purpose of the Navier-Stokes equations, the three dimensional axis is orientated from the center of the oscillating disk.

Several assumptions can be made to simplify equation (30) further:

1. Since $h \ll R$ (or $z \ll x$ and $z \ll y$), non-dimensionalizing the equation variables shows that the rate of change of velocities with respect to the x– and y–directions will be negligible when compared to the rate of change of the velocities in the z–direction on the right side of equation (30).

2. The Reynolds number, $\mathrm{Re} \approx \frac{\rho U L}{\mu}$, is small for most MEMS devices ($\mathrm{Re} \ll 1$), with U and L representing the characteristic velocity and length. Since,

$$\mathrm{Re} \approx \frac{\rho \vec{V}\left(\nabla \vec{V}\right)}{\mu \nabla^2 \vec{V}} \approx \frac{\rho u \frac{\partial u}{\partial x}}{\mu \frac{\partial^2 u}{\partial z^2}}, \tag{31}$$

   the time-independent convection term $\rho \vec{V}\left(\nabla \vec{V}\right)$ can be neglected.

3. Since $h \ll r$, it can be shown that the non-dimensionalized partial differential $\frac{\partial p'}{\partial z'}$ is one order smaller than $\frac{\partial p'}{\partial x'}$, or $\frac{\partial p'}{\partial y'}$, and with $\frac{\partial z}{\partial t} = w = 0$ for lateral oscillations, the entire z–direction momentum equation can be neglected.

The application of these assumptions is detailed in Appendix D. Using the above assumptions, the Navier-Stokes equation can be reduced to the form

$$x - \text{component} \qquad \rho \frac{du}{dt} + \frac{\partial p}{\partial x} = \mu \frac{\partial^2 u}{\partial z^2} \tag{32a}$$

$$y - \text{component} \qquad \rho \frac{dv}{dt} + \frac{\partial p}{\partial y} = \mu \frac{\partial^2 v}{\partial z^2}. \tag{32b}$$

Consider the $x-$component equation (32b). Depicting general radial displacement to be $de^{i\omega t}$ will give us real radial velocity of $U = d\omega e^{i\omega t}$. For the current geometry, d is designated to be of order 10^{-9}, $h = 1$ micron and disc radius, $R = 10$ microns. Non-dimensionalizing and with U and h and taking their ratio gives,

$$\frac{\rho \frac{\partial u}{\partial t}}{\mu \frac{\partial^2 u}{\partial z^2}} = \frac{\rho h^2}{\mu T} \frac{\rho \frac{\partial u'}{\partial t'}}{\mu \frac{\partial^2 u'}{\partial z'^2}} \approx \frac{\rho h^2}{\mu T} = \frac{\rho h^2 d\omega}{\mu R} \tag{33}$$

since the non-dimensionalized derivative terms are now comparable and the period is $T \approx R/U$ for the geometry. Substituting values of h, d, R, $\rho = 1.17\ \frac{kg}{m^3}$ and $\mu = 0.1848 \times 10^{-4}$

$\frac{kg}{m\,sec}$ for air and letting $\frac{\rho h^2 d\omega}{\mu R}$ equal 1 to make the numerator and denominator comparable, it is calculated that ω has to be of at least order 10^{12} Hz for the latter to be true. Since ω is of order 10^9 Hz for the current geometry, $\rho\frac{\partial u}{\partial t}$ can be neglected. The same argument can be applied to the y-component of the gas-film equations and the final governing equations result to,

$$x-\text{component} \qquad \frac{\partial p}{\partial x} = \frac{\partial}{\partial z}\left(\mu\frac{\partial u}{\partial z}\right) \tag{34a}$$

$$y-\text{component} \qquad \frac{\partial p}{\partial y} = \frac{\partial}{\partial z}\left(\mu\frac{\partial v}{\partial z}\right) \tag{34b}$$

The variables u, v and p in equation (34) can be solved using the third equation provided by the continuity condition as will be seen later.

Current geometry implicitly implies fluid velocity at $z = h$ to be $u = U(x, y)e^{i\omega t}$ in the x–direction and $v = V(x, y)e^{i\omega t}$ in the y–direction and at $z = 0$ to be $u = v = 0$. By inspection, fluid velocity at varying z is $u = \tilde{U}(x, y, z)e^{i\omega t}$ and $v = \tilde{V}(x, y, z)e^{i\omega t}$ respectively. Furthermore, pressure can be most generally depicted as $p = P(x, y)e^{i\omega t}$ and density as $\rho = \tilde{\rho}(x, y)e^{i\omega t}$ considering a very small h. Substituting $u = \tilde{U}(x, y, z)e^{i\omega t}$ and $v = \tilde{V}(x, y, z)e^{i\omega t}$ into equation (34a) gives,

$$\frac{\partial}{\partial z}\left(\mu\frac{\partial \tilde{U}}{\partial z}\right) = \frac{\partial P}{\partial x}$$

Performing an integral from $z = 0$ to z yields,

$$\mu\frac{\partial \tilde{U}}{\partial z} - \mu\left.\frac{\partial \tilde{U}}{\partial z}\right|_{z=0} = \frac{\partial P}{\partial x}z$$

and another similar integral gives,

$$\mu\tilde{U} - \mu\left.\frac{\partial \tilde{U}}{\partial z}\right|_{z=0} z - \left.\mu\tilde{U}\right|_{z=0} = \frac{1}{2}\frac{\partial P}{\partial x}z^2 \tag{35}$$

Using equation (35) and the necessary boundary condition of $\tilde{U} = 0$ at $z = 0$, we have

$$\left.\mu\tilde{U}\right|_{z=0} = 0. \tag{36}$$

Using the boundary condition $\tilde{U} = U$ at $z = h$ in equation (35), the second integration constant is found to be

$$\mu\left.\frac{\partial \tilde{U}}{\partial z}\right|_{z=0} = \frac{\mu U}{h} - \frac{h}{2}\frac{\partial P}{\partial x} \tag{37}$$

Substituting equation (37) back into equation (35) gives equation (38a),

$$\tilde{U} = \frac{z}{h}U + \frac{1}{2\mu}\frac{\partial P}{\partial x}z\left(z-h\right) \tag{38a}$$

$$\tilde{V} = \frac{z}{h}V + \frac{1}{2\mu}\frac{\partial P}{\partial y}z\left(z-h\right) \tag{38b}$$

with a similar result (38b) for the y–direction. The continuity condition from equation (29) can be reduced to

$$\frac{\partial\left(\tilde{\rho}\tilde{W}\right)}{\partial z} = -\frac{\partial\left(\tilde{\rho}\tilde{U}\right)}{\partial x} - \frac{\partial\left(\tilde{\rho}\tilde{V}\right)}{\partial y} \tag{39}$$

with the assumption that the squeeze film enclosure is tight enough to prevent the escape of fluid thus maintaining a constant fluid mass. Furthermore, the change in volume of the enclosure can be neglected due to minute perturbation. Taking an integral with respect to z eliminates the z–component of equation (39) since geometrical constraints ensure only lateral motion. The ensuing equation results as,

$$0 = \int_0^h -\frac{\partial\left(\tilde{\rho}\tilde{U}\right)}{\partial x} - \frac{\partial\left(\tilde{\rho}\tilde{V}\right)}{\partial y}\partial z. \tag{40}$$

Substituting equation (38a) and (38b) into equation (40) and performing the integral yields

$$\frac{\partial\left(\tilde{\rho}U\right)}{\partial x} + \frac{\partial\left(\tilde{\rho}V\right)}{\partial y} = \frac{h^2}{6\mu}\left[\frac{\partial}{\partial x}\left(\tilde{\rho}\frac{\partial P}{\partial x}\right) + \frac{\partial}{\partial y}\left(\tilde{\rho}\frac{\partial P}{\partial y}\right)\right]. \tag{41}$$

Using the ideal gas assumption that $P/\rho =$ constant, the above becomes

$$\frac{\partial\left(PU\right)}{\partial x} + \frac{\partial\left(PV\right)}{\partial y} = \frac{h^2}{6\mu}\left[\frac{\partial}{\partial x}\left(P\frac{\partial P}{\partial x}\right) + \frac{\partial}{\partial y}\left(P\frac{\partial P}{\partial y}\right)\right]. \tag{42}$$

Analysis of the finite element results of a modal analysis of the disk geometry yielded relations for the $x-$ and $y-$components of the fluid velocity field for a vibrational mode that would result in various geometry deformations in the range of the operating frequency The amplitudes of the velocity components in these cases are give in Table 5.2 $U = r\cos(\theta)$ and $V = -r\sin(\theta)$, where $r = \sqrt{x^2+y^2}$, $\cos(\theta) = x/r$, and $\sin(\theta) = y/r$, or $U = x$ and $V = -y$.

Mode Shape	Velocity Components
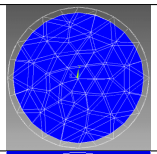	$U = \frac{R}{10}\cos(\theta)$ $V = \frac{R}{10}\cos(\theta)$
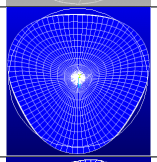	$U = \frac{2x}{25}\cos(3\theta)$ $V = \frac{2y}{25}\cos(3\theta)$
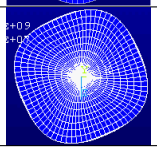	$U = \frac{2x}{15}\cos(4\theta)$ $V = \frac{2y}{15}\cos(4\theta)$

5.3 Numerical Study and Results

Using the FEMLAB finite element application extension for MATLAB, a solution to equation (42) was found. The boundary condition for the analysis was that $P - P_a = 0$, where P_a is the atmospheric pressure (101.325 kPa). FEMLAB produced $P = P_a$ as a solution to Equation (13) for the conditions specified. This is a valid solution in that the right-hand side of the equation goes to zero and the sum of the partial derivatives $\partial U/\partial x$ and $\partial V/\partial y$ is also zero. As the frequency of the applied voltage increases, the vibrational modes of the disc will change. The next section discusses the analysis of the disc geometry to determine other vibrational modes that might occur in the 0.4×10^8 to 1.0×10^9 Hz frequency range.

The results show that for a maximum velocity of unity, there is only a very small pressure perturbation at the solid-gas interface. The order of the greatest change in pressure is 10^{-4}, which is very small when compared to the order of the pressure (10^5). Because of this, it can be said that for this resonator case, the effects of the compressibility of the gas film between the device and the substrate will be negligible. This means that the damping in this layer can be simulated using the incompressible Navier-Stokes flow equations.

Pressure Contours	Pressure Results
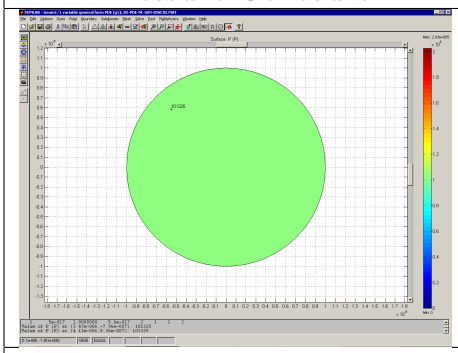	$P = P_0$
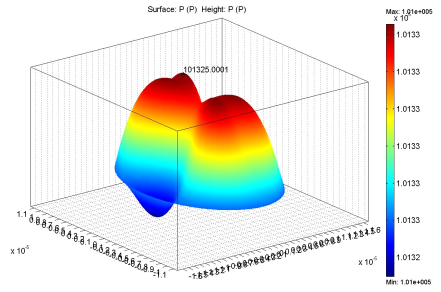	$P_{min} = 1.013249999697598 \times 10^5$ Pa $P_{max} = 1.013250001056202 \times 10^5$ Pa $\delta P_{max} = 1.056202308973298 \times 10^{-4}$ Pa
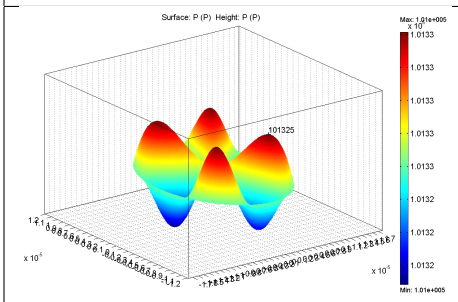	$P_{min} = 1.013250000679355 \times 10^5$ Pa $P_{max} = 1.013249999403262 \times 10^5$ Pa $\delta P_{max} = 6.793547072447836 \times 10^{-4}$ Pa

CHAPTER VI

CONCLUSIONS AND FUTURE WORK

6.1 Conclusions

6.1.1 Investigation of Existing Analytical Models

An investigation into the two molecular dynamics approaches to the air damping of a resonating beam was brought forth in this work. Errors and limitations of these methods were discussed in detail. It was found that Christian's free molecular model, while valid for a gas in equilibrium, was not suitable for use in studying devices that operate in confined areas. It was also found that the work by Kadar and Li to improve the free molecular model was in error because of the modified gas velocity distribution function was applied incorrectly to Christian's model and the derivation of this function was not correct for the system conditions. The second model that was investigated was Bao's energy transfer model. This model uses the energy and momentum transfer between the molecules and the moving structure to determine the energy dissipation. The energy transfer model also accounts for the presence of nearby walls. It was because of these characteristics that this model was singled out for further analysis. The analysis revealed that the model was based on three assumptions. These were that the velocity of the molecule can be treated as constant throughout its interaction with the moving structure, the travel time of the molecule was much smaller than the oscillation period of the moving structure, and the amplitude of the structure's oscillation was small enough to consider the displacement of the beam as negligible. These assumptions lead to an underestimation of the energy dissipation, which results in an over-approximation of the device's quality factor.

6.1.2 Molecular Dynamics Simulation

A molecular dynamics simulation code was developed to model the energy dissipation for a general beam resonator. The code was used to verify Bao's assumptions by achieving results

that were less than 1% different than the analytical solution. The results from the code were then compared to existing experimental results, and were found to have very good agreement in the free molecular regime. With this validation, the code was then used to investigate the effects of the oscillation mechanics on the behavior of the beam. While investigating the gap-to-amplitude ratio dependence, it was found that as the amplitude of oscillation increases, the energy dissipation decreases, but the quality factor is strongly effected when the ratio is small and nearly unaffected when the ratio is large. While evaluating the dependence of the energy dissipation and quality factor on the Stokes number, it was found that the energy dissipation and quality factor decrease with decreasing frequency. It was also found that there is a linear dependence of the energy dissipation and quality factor on the pressure and the frequency when the frequency is less than 3 MHz.

6.1.3 Compressibility Effects Study

The compressibility effects of a 1 micron thick film of air on a laterally-oscillating disk resonator were investigated. This work involved the application and reduction of the Navier-Stokes flow equations. Once a reduced form was obtained, the finite element analysis software FEMLAB was used to solve the resulting nonlinear partial differential equation. For various disk velocity profiles, it was shown that the pressure perturbation was minimal. This means that the compressibility effects in this case were negligible and that the incompressible form of the Navier-Stokes equations could be used to solve for the behavior of the flow.

6.2 Future Work

Due to the limitations of the molecular dynamics code, it is difficult to apply it to more general cases. A simulation technique that can account for several domain boundary conditions, as well as multiple particles and particle types, is needed. One such technique is the direct simulation Monte Carlo (DSMC) method. This simulation is a stochastic direct particle simulation method that is based on kinetic theory. A large number of statistically representative particles are tracked during the simulation, instead of all the particles as in conventional molecular dynamics (MD) simulations. The motion of these particles and their

interactions are then used to modify their positions, velocities, or drive chemical reactions. The laws of conservation of mass, momentum and energy are enforced to maintain accuracy.

The DSMC method uncouples the molecular motion and interactions with the boundaries from the intermolecular collisions. This is done over very small time intervals, on the order of the mean free time of the gas. As a result of this, the amount of computation required is proportional to N (the number of molecules), in contrast to N^2 for MD simulations. In essence, particle motions are modeled deterministically while collisions are treated probabilistically, each simulated molecule representing a large number of actual molecules. The DSMC method is discussed in detail in the literature [3, 9].

There is currently a DSMC code under development in the Complex Systems Design Automation (CSDA) group in the mechanical engineering department at Georgia Tech. The code is being developed as a modeling technique for the design of thermal sensing atomic force microscopes (AFM). This code is currently under modification for application to the case of a MEMS resonator, where a solid wall is treated as if it were oscillating by imposing a sinusoidal velocity and position. Particles that interact with the wall either gain or lose velocity based on the phase of the oscillation. The effects of the sinusoidal input are similar to those for sound wave propagation [12, 11, 27]. To test the accuracy of the simulation, a case was chosen such that the results could be compared with existing continuum models. Figure 6.2 shows the two-dimensional simulation domain along with the chosen boundary conditions.

Table 7: DSMC Simulation Parameters and Boundary Conditions

Simulation Parameters	**Air Properties**	**Boundary Conditions**
$P = 101325$ Pa	$\mu = 1.73\text{e}{-5}$ Pa-sec	$X = 0$, Moving Wall
$T = 273$ K	$d_{gas} = 3.5887\text{e}{-10}$ m	$X = d_0$, Thermal Wall
$f = 10e9$ Hz	$m = 4.80895\text{e}26$ kg	$Y = 0$, Specular
$d_0 = 1\text{e}{-6}$ m	$\rho = 1.29$ kg/m^3	$Y = L_x$, Pressure
$L_x = 5\text{e}{-6}$ m		
$G/A = 100$		

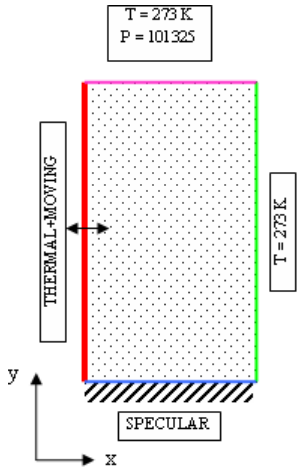

Figure 22: DSMC Simulation Boundary Conditions

The simulation was run for several oscillation cycles (at least 500), in the hopes of capturing the system's behavior when it reaches an equilibrium state. The calculated quality factor using the Pressure Inlet boundary condition was 9.66e9 and 1.01e10 for the Pressure Outlet boundary condition. The preliminary results for this case are of the same magnitude as those obtained using the isothermal squeeze film calculations (7.39e9) [4]. While preliminary results have been obtained, they have led to a closer investigation of the calculation of boundary interactions.

APPENDIX A

DEFINITION OF TERMS

Many terms have been referenced throughout this study. Some important terms are defined below [26]:

Damping	Dissipation of oscillatory or vibratory energy with motion or with time
Density	Ratio of the mass of a substance to the volume it occupies
Mean Free Path	Average distance which a molecule travels in a gas before it collides with another molecule
Molecule	The smallest particle of a substance which will still retain the essential composition and properties of that substance
Quality Factor	The ratio of the total energy input into the device to the energy dissipated within a finite space of time
Knudsen Number	The ratio of of the mean free path of a gas molecule to the characteristic length of the flow
Radio Frequency	A frequency at which coherent electromagnetic radiation of energy is useful for communications. Radio frequencies are designated as very low: <30 kHz, low: 30 to 300 kHz, medium: 300 to 3,000 kHz, high: 3 to 30 MHz, very high: 30 to 300 MHz, ultrahigh: 300 to 3,000 MHz, superhigh: 3 to 30 GHz, and extremely high: 30 to 300 GHz
Resonator	Device with a vibratory natural response
Oscillator	Resonator plus an external circuit that provides the energy to sustain steady-state oscillation
Viscous	Resistant to flow under stress

APPENDIX B

MOLECULAR DYNAMICS SIMULATION CODE

Molecular Dynamics Simulation Code: Second Variation

by Sarne M. Hutcherson

written in C++

```
#include <cstdlib>
#include <math.h>
#include <iostream>
#include <iomanip>
#include <fstream>
#include <string>
#include <direct.h>


using namespace std;

// Constants ------------------------------------------------
const double BEAM_THICKNESS = 1.8e-6;
const double BEAM_GAP = 1.1e-6;
const double BEAM_WIDTH = 40e-6;
const double BEAM_LENGTH = 200e-6;
const double BEAM_FREQUENCY = 550e3;
const double NA = 6.022e23;
const double Mm = 0.02896;
const double R = 8.31447;
const double TEMP = 273;
const double BOLTZ = 1.3807e-23;
const double PI = 3.14159265359;
const double RHO = 1.29;
const double P0 = 101325;
const double RHO_SI = 2330;
const double AVERAGE_VELOCITY = sqrt( 8 * R * TEMP / ( Mm * PI ) );
const double DENS_CONST = 0.25 * AVERAGE_VELOCITY * (2*BEAM_LENGTH + 2*BEAM_WIDTH) / (Mm / NA);

double qf_data[4];
double num_part[2];

struct particleRec
{
  double  velocity;
  double  position;
  double  changev;
  double  time;
  double  kinetic;
}particle;

struct beamRec
{
  double  velocity;
  double  vel_avg;
  double  position;
  double  pos_avg;
  double  time;
  double  frequency;
}beam;


struct simRec
{
  double  step;
  double  endtime;
  double  time;
  double  dv;
  double  offset;
}sim;

struct energyRec
{
  double  inst_energy;
  double  ave_energy;
  double  sum_energy;
```

```
  double  deltav2;
  int     collisions;
  double  num_density;
  double  corrected;
}energy;


double quality_factor(double aa, double bb, double A0, double a_const, double omega, double time, double energy_sim, double rho_)
{
  double  number_density = rho_ /( Mm / NA );
  double  energy_beam = 2 * PI * 0.5 * RHO_SI * BEAM_THICKNESS * bb * aa * omega * omega * A0 * A0;

  num_part[0] = 0.25 * number_density * AVERAGE_VELOCITY * A0 * a_const * 2 * (aa + bb);
  num_part[1] = 0.25 * number_density * AVERAGE_VELOCITY * A0 * a_const * 2 * (aa + bb) * time;

  // Energy Transferred from Beam during Simulation
  qf_data[0] = 0.25*number_density*AVERAGE_VELOCITY
    *A0*a_const*(2 * bb + 2 * aa) * energy_sim *time;
  // Quality Factor of Beam from Simulation
  qf_data[1] = energy_beam/qf_data[0];
  // Energy Transferred from Beam from Bao's Theory
  qf_data[2] = (PI/16)*rho_*AVERAGE_VELOCITY*(2*aa*bb/PI)
    *A0*A0*omega*(2*aa + 2*bb)/(A0*a_const);
  // Quality Factor of Beam from Bao's Theory
  qf_data[3] = energy_beam/qf_data[2];

  return energy_beam;
}

void main()
{
  int     i, perdiv, N;
  int     J, K, k, num_coll[3], coll_beam[3]; // L,
  double  travel_time, Xi;
  double  aa = BEAM_LENGTH, bb = BEAM_WIDTH, t;
  double  d = BEAM_GAP, A0, a_const, omega, pressure, rho_, dfrac;
  double  m, Vyi, Vzi, Vyz, Vxi, Vxf, v, v2[3], l, initV;
  double  position_check[3], energy_beam;
  char    name_holder[90];

  ofstream fname3;
  ofstream summary;
  ofstream divstats;

  fname3 <<scientific <<setprecision(10);
  summary <<scientific <<setprecision(10);
  divstats <<scientific <<setprecision(10);

  beam.frequency = BEAM_FREQUENCY;

  sim.dv = 0;
  m = Mm/NA;
  J = 1;

  _mkdir("DATA_BAO_NAnB1");

  cout    <<"Simulation:\tBeam_Bao_NAnB1" << endl;
  cout    <<"Enter the number of period divisions:           ";
  cin     >>perdiv;
  cout    <<"Enter the frequency:                            ";
  cin     >>beam.frequency;
  omega = 2*PI*beam.frequency;
  cout    <<"Enter the amplitude scale:                      ";
  cin     >>a_const;
  A0 = d/a_const;
  cout    <<"Enter the pressure:                             ";
  cin     >>pressure;
  rho_ = RHO*pressure/P0;
  cout    <<"Enter the starting location coefficient (0-1):  ";
  cin     >>dfrac;
  cout    <<"Enter the number of particles per division:     1";
  N = 1;

  energy.sum_energy = 0;
  energy.collisions = 0;
  energy.deltav2 = 0;

  i = sprintf(name_holder, "DATA_BAO_NAnB1\\summary_pd%d_a%d_f%d_pr%d_s%d.txt",
    perdiv,(int)a_const,(int)beam.frequency,(int)pressure,(int)(dfrac*100));
  summary.open(name_holder);

  i = sprintf(name_holder, "DATA_BAO_NAnB1\\divstats_pd%d_a%d_f%d_pr%d_s%d.txt",perdiv,
    (int)a_const,(int)beam.frequency,(int)pressure,(int)(dfrac*100));
  divstats.open(name_holder);
  divstats <<
    "#K\tperdiv\ttime\tVxi\tVxf\tDV\tD(VV)\tCollisions"
    << "\tEnergy\tCumm. Energy\t\tBAP\tBAV" << endl;

  beam.time = 1/beam.frequency;
  sim.offset = beam.time/perdiv;

  particle.velocity = sqrt(0.33333333333333*AVERAGE_VELOCITY*AVERAGE_VELOCITY);
```

```
Vyi = particle.velocity;
Vzi = particle.velocity;
Vyz = sqrt(Vyi * Vyi + Vzi * Vzi);

Vxi =  particle.velocity;

l = sqrt(2*aa*bb/PI);
travel_time = l/Vyz;
particle.time = min(travel_time,beam.time);

cout << endl;

for(K = 0; K <= perdiv; K++)
{
  if(K%50<1)
  {
    cout << K << "\t" << K << "\t" << K
      << "\t" << K << "\t" << K << "\n";
  }

  energy.ave_energy = 0;
  energy.inst_energy = 0;

  particle.changev = 0;
  particle.kinetic = 0;

  beam.position = BEAM_GAP;
  beam.pos_avg = 0;
  beam.velocity = 0;
  beam.vel_avg = 0;

  sim.time = sim.offset * K;
  sim.endtime = particle.time + sim.offset*K;
  sim.step = particle.time / 50000;

  num_coll[0] = 0;

  initV = Vxi;
  if((dfrac>=0)||(dfrac<=1))
  { Xi = dfrac*BEAM_GAP;}
  else
  { Xi = 0;}

  particle.position = Xi;
  particle.changev = 0;
  particle.velocity = abs(Vxi);

  t = sim.time;

  coll_beam[0] = 0;

  k = 0;

  while (sim.endtime > sim.time)
  {
    sim.time = sim.offset * K + sim.step * k;
    k = k + 1;
    //NO CONSTANT BEAM VELOCITY
    beam.velocity = A0*omega*cos(omega*sim.time);
    beam.vel_avg += beam.velocity;
    //NO CONSTANT BEAM POSITION
    beam.position = BEAM_GAP-A0*sin(omega*sim.time);
    beam.pos_avg += beam.position;

    particle.position = particle.position + particle.velocity*sim.step;
    position_check[0] = beam.position - particle.position;

    if(particle.position < 0)
    {
      num_coll[0] = num_coll[0] + 1;
      particle.velocity = -(particle.velocity);
    }
    else if(position_check[0] < 0 && particle.position > 0 && particle.velocity > 0)
    {
      num_coll[0] = num_coll[0] + 1;
      coll_beam[0] = coll_beam[0] + 1;
      particle.changev = particle.changev + 2*beam.velocity;
      //NO CONSTANT PARTICLE VELOCITY
      particle.velocity = -(particle.velocity + 2*beam.velocity);
    }
    else
    {
      particle.velocity = particle.velocity;
    }
  }

  Vxf = abs(particle.velocity);
  v = abs(Vxf) - abs(Vxi);
  v2[0] = Vxf*Vxf - Vxi*Vxi;
  sim.dv = sim.dv + v2[0];

  energy.deltav2 = energy.deltav2 + v2[0];
```

```
    energy.inst_energy = v2[0]*m*(0.5);
    energy.ave_energy = energy.ave_energy + energy.inst_energy;
    energy.collisions = energy.collisions + coll_beam[0];

    particle.kinetic = energy.inst_energy;

    beam.pos_avg = beam.pos_avg/k;
    beam.vel_avg = beam.vel_avg/k;

    energy.sum_energy = energy.sum_energy + (energy.ave_energy/N);
    energy.num_density = DENS_CONST * rho_ * beam.pos_avg * sim.offset;
    energy.corrected += energy.ave_energy * energy.num_density;

    divstats << K << '\t' << perdiv << '\t' << sim.offset
      << '\t' << Vxi << '\t' << Vxf << '\t' << particle.changev
      << '\t' << energy.deltav2 << '\t' << coll_beam[0] << '\t'
      << energy.inst_energy << '\t' << energy.sum_energy << "\t\t" << beam.pos_avg
      << '\t' << beam.vel_avg << '\t' << energy.num_density << '\t'
      << (energy.sum_energy*energy.num_density) << endl;
  }

  energy_beam = quality_factor(aa,bb,A0,a_const,omega,sim.offset,energy.sum_energy,rho_);

  divstats << endl << "The theoretical quality factor is:  \t" << qf_data[3];
  cout << endl << "The theoretical quality factor is:  \t" << qf_data[3];
  divstats << endl << "The quality factor of the device is:\t" << qf_data[1];
  cout << endl << "The quality factor of the device is:\t" << qf_data[1];
  divstats << endl << "The quality factor (corrected) of the device is:\t"
    << energy_beam/energy.corrected;
  cout << endl << "The quality factor (corrected) of the device is:\t"
    << energy_beam/energy.corrected;

  summary << endl << "Simulation:\tBEAM_BAO_NAnB1" << endl
    << "Number of Period Divsions:\t" << perdiv << endl
    << "Number of Particles per division:\t" << N << endl
    << "Operating Frequency:\t" << beam.frequency << endl
    << "Amplitude:\t" << A0 << endl
    << "Pressure:\t" << pressure << endl
    << "Starting Position:\t" << dfrac*BEAM_GAP << endl << endl
    << "Energy Transferred from Device to Gas for " << ((perdiv+1)*N)
    << " particles:\t" << energy.sum_energy << endl << endl
    << "Average d(V^2) for particles:\t" << (energy.deltav2/N) << endl
    << "Total Number of Collisions with Device:\t" << energy.collisions
      << endl << endl << endl
    << "Total Number of Particles entering Region per Second:\t"
      << num_part[0] << endl
    << "Total Number of Particles entering per Period Divisoin:\t"
      << num_part[1] << endl << endl
    << "The total energy for one cycle:\t" << qf_data[0] << endl
    << "The quallity factor for this device:\t" << qf_data[1] << endl
    << "The quality factor (corrected) of the device is:\t" << energy_beam/energy.corrected << endl
    << "The total theoretical energy for one cycle:\t" << qf_data[2] << endl
    << "The theoretical quality factor is:\t" << qf_data[3];

  summary.close();
  divstats.close();
  cout << "\a\a";
}
```

APPENDIX C

RANDOM MAXWELL-BOLTZMANN VELOCITY GENERATOR

C.1 The Inverse Method

Given a continuous distribution function $P(x)$, you can generate numbers according to this distribution using a uniform random number generator. For $P(x)$, there exists a function $D(x')$ such that

$$D(x') \equiv \int^{x'} P(x)dx$$

If the random number generator produces numbers of value y in the range $[0, 1]$, $P(x)$ can be connected to y by

$$x_i = D^{-1}(y_i),$$

where $D^{-1}(y_i)$ is the inverse of the function $D(x')$.

C.2 Maxwell-Boltzmann Number Generator

Given the Maxwell-Boltzmann velocity distribution function

$$P(x) = MB(v) = \left(\frac{m}{2\pi kT}\right)^{\frac{1}{2}} \exp\left(-\frac{mv^2}{2kT}\right),$$

Using the property $erf(z) \equiv \frac{2}{\sqrt{\pi}} \int_0^z e^{-t^2} dt$, $D(x)$ will become

$$\begin{aligned} D(x) &= \int^x \left(\frac{m}{2\pi k_B T}\right)^{\frac{1}{2}} \exp\left(-\frac{mv^2}{2k_B T}\right) dv, \text{ let } a = \frac{m}{2k_B T} \\ &= \int^x \left(\frac{a}{\pi}\right)^{\frac{1}{2}} \exp\left(-av^2\right) dv \\ &= \left(\frac{1}{\pi}\right)^{\frac{1}{2}} \int^x \exp\left(-t^2\right) dt = \left(\frac{1}{\pi}\right)^{\frac{1}{2}} \left(\frac{\sqrt{\pi}}{2} \operatorname{erf}(x)\right) \\ &= \frac{1}{2}\operatorname{erf}\left(\sqrt{\frac{m}{2k_B T}}\, v\right). \end{aligned}$$

The inverse $D^{-1}(x)$ of $D(x)$ can then be found as

$$D^{-1}(y_i) = v_{xi} = \sqrt{\frac{2k_BT}{m}}\,\text{erfinv}(2y_i - 1),$$

where y_i is a number supplied from a uniform random number generator. The argument to erfinv(...) was changed to reflect both the positive and negative halves of the velocity distribution function. Inspection of the relation for v_{xi} shows that the produced random velocity is based on the most probable velocity of the gas molecules. In Figure C.2, the graph on the left is a graph of the Maxwell-Boltzmann velocity distribution function. The graph on the right shows a histogram of $100,000$ numbers generated using the v_{xi} relation and a uniform random number input for y_i.

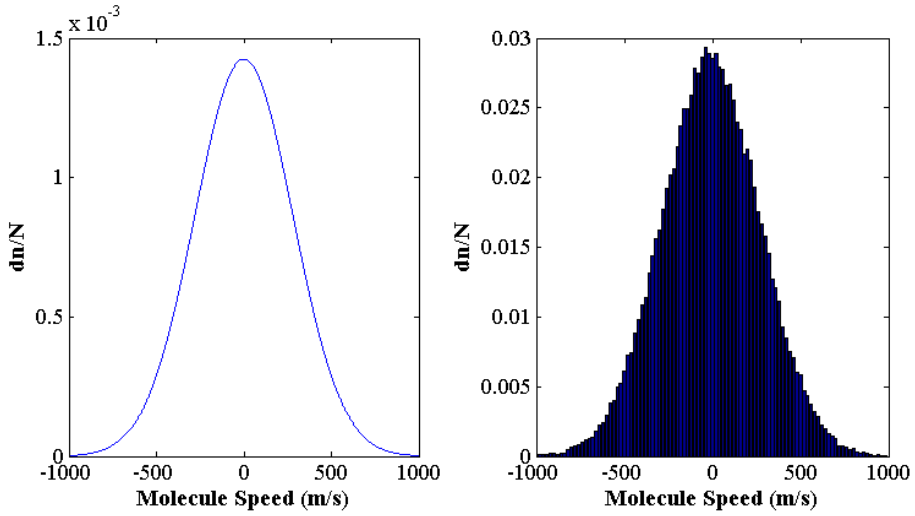

The Maple validation of this derivation is provided below:

```
> g:=sqrt(m/2/pi/k/T)*exp(-m*(v)^2/2/k/T);
```

$$g := \frac{1}{2}\sqrt{2}\sqrt{\frac{m}{\pi\,k\,T}}\,e^{(-1/2\,\frac{m\,v^2}{k\,T})}$$

```
> dd := int(g,v);
```

$$dd := \frac{1}{2}\,\frac{\sqrt{\frac{m}{\pi\,k\,T}}\,\sqrt{\pi}\,\text{erf}(\frac{1}{2}\,\sqrt{2}\,\sqrt{\frac{m}{k\,T}}\,v)}{\sqrt{\frac{m}{k\,T}}}$$

```
> simplify(dd);
```

$$\frac{1}{2}\,\frac{\sqrt{\frac{m}{\pi\,k\,T}}\,\sqrt{\pi}\,\text{erf}(\frac{1}{2}\,\sqrt{2}\,\sqrt{\frac{m}{k\,T}}\,v)}{\sqrt{\frac{m}{k\,T}}}$$

```
> y:=solve(x=dd,v);
```

$$y := \frac{\mathrm{RootOf}(-\mathrm{erf}(\_Z)\sqrt{\frac{m}{\pi\,k\,T}}\,\sqrt{\pi} + 2\,x\,\sqrt{\frac{m}{k\,T}})\,\sqrt{2}}{\sqrt{\frac{m}{k\,T}}}$$

Solving $\mathrm{RootOf}(-\mathrm{erf}(\_Z)\sqrt{\frac{m}{\pi\,k\,T}}\,\sqrt{\pi} + 2\,x\,\sqrt{\frac{m}{k\,T}})$**, by inspection, for** $\_\mathbf{Z} = \mathbf{Z}$**:**

```
> Z := erfinv(2*x);
```

```
> yy := Z*2^(1/2)/(m/k/T)^(1/2);
```

$$Z := \mathrm{erfinv}(2\,x)$$

$$yy := \frac{\mathrm{erfinv}(2\,x)\,\sqrt{2}}{\sqrt{\frac{m}{k\,T}}}$$

```
> v_i = expand(yy);
```

$$v\_i = \frac{\mathrm{erfinv}(2\,x)\,\sqrt{2}}{\sqrt{\frac{m}{k\,T}}}$$

Also, to investigate the effects of an additional normal velocity component, as in the case of a moving wall, the Maple result was modified to solve for the distribution of molecules with velocities of $v + u$. It can be seen from the result that the magnitude of the moving wall's velocity is unchanged through the transformation. Only its sign is changed. This is most likely due to the assumption that initially the wall and molecule are moving toward one another.

```
> g:=sqrt(m/2/pi/k/T)*exp(-m*(v+u)^2/2/k/T);
```

$$g := \frac{1}{2}\,\sqrt{2}\,\sqrt{\frac{m}{\pi\,k\,T}}\,e^{(-1/2\,\frac{m\,(v+u)^2}{k\,T})}$$

```
> dd := int(g,v);
```

$$dd := \frac{1}{2}\,\frac{\sqrt{\frac{m}{\pi\,k\,T}}\,\sqrt{\pi}\,\mathrm{erf}\left(\frac{1}{2}\,\sqrt{2}\,\sqrt{\frac{m}{k\,T}}\,v + \frac{\frac{1}{2}\,m\,u\,\sqrt{2}}{k\,T\,\sqrt{\frac{m}{k\,T}}}\right)}{\sqrt{\frac{m}{k\,T}}}$$

```
> simplify(dd);
```

$$\frac{1}{2}\,\frac{\sqrt{\frac{m}{\pi\,k\,T}}\,\sqrt{\pi}\,\mathrm{erf}\left(\frac{1}{2}\,\frac{\sqrt{2}\,m\,(v+u)}{k\,T\,\sqrt{\frac{m}{k\,T}}}\right)}{\sqrt{\frac{m}{k\,T}}}$$

```
> y:=solve(x=dd,v);
```

$$y := \frac{1}{2}\,\frac{(-m\,u\,\sqrt{2}+2\,\mathrm{RootOf}(-\mathrm{erf}(\_Z)\,\sqrt{\frac{m}{\pi\,k\,T}}\,\sqrt{\pi}+2\,x\,\sqrt{\frac{m}{k\,T}})\,k\,T\,\sqrt{\frac{m}{k\,T}})\,\sqrt{2}}{m}$$

Solving $\mathrm{RootOf}(\mathrm{erf}(\_Z)\,\sqrt{\frac{m}{\pi\,k\,T}}\,\sqrt{\pi}-2\,x\,\sqrt{\frac{m}{k\,T}})$**, by inspection, for _Z = Z:**

```
> Z := erfinv(2*x);
```

```
> yy := -1/2*(m*u*sqrt(2)-2*Z*k*T*sqrt(m/k/T))*2^(1/2)/m;
```

$$Z := \mathrm{erfinv}(2\,x)$$

$$yy := -\frac{1}{2}\,\frac{\left(m\,u\,\sqrt{2}-2\,\mathrm{erfinv}(2\,x)\,k\,T\,\sqrt{\frac{m}{k\,T}}\right)\,\sqrt{2}}{m}$$

```
> v_i = expand(yy);
```

$$v\_i = -u+\frac{\sqrt{2}\,\mathrm{erfinv}(2\,x)\,k\,T\,\sqrt{\frac{m}{k\,T}}}{m}$$

APPENDIX D

SLIDE-FILM DAMPING ANALYSIS: SIMPLIFICATION ASSUMPTIONS

D.1 Non-Dimensionalization of the Navier-Stokes Equations for a Laterally-Oscillating Disk Resonator

For MEMS devices, the Reynold's number is generally very small, i.e. Re $\ll 1$. For this case, the characteristic velocity U for the geometry that would result in such a small Reynolds number must be very small itself. Since

$$\mathrm{Re} \approx \frac{\rho\vec{V}\left(\nabla\vec{V}\right)}{\mu\nabla^2\vec{V}},$$

the $\rho\vec{V}\left(\nabla\vec{V}\right)$ convection term will have little effect when compared with the viscosity term, $\mu\nabla^2\vec{V}$, that is $\rho\vec{V}\left(\nabla\vec{V}\right) \ll \mu\nabla^2\vec{V}$, thus allowing the convection term's elimination from equation (30), leaving

$$\rho\frac{d\vec{V}}{dt} = -\nabla P + \mu\nabla^2\vec{V} + \frac{\mu}{3}\nabla\left(\nabla \bullet \vec{V}\right) + \rho\vec{b}$$

It is also assumed that the body force within the fluid is negligible, or $\rho\vec{b} = 0$. The equation now reduces to

$$\rho\frac{d\vec{V}}{dt} = -\nabla P + \mu\nabla^2\vec{V} + \frac{\mu}{3}\nabla\left(\nabla \bullet \vec{V}\right) \tag{43}$$

In order to further reduce the momentum equation, the equation variables were non-dimensionalized using the following:

$$\bar{V}' = \bar{V}/U,\ x' = x/L,\ y' = y/L,\ z' = z/h,\ p' = P\Big/\rho U^2,\ T = L/U,\ t' = t/T = tU/L$$

Substituting the above into the x-component of equation (43) yields

$$\rho\left(\frac{U^2}{L}\frac{\partial u'}{\partial t'} + \frac{U^2u'}{L}\frac{\partial u'}{\partial x'} + \frac{U^2v'}{L}\frac{\partial u'}{\partial y'} + \frac{U^2w'}{L}\frac{\partial u'}{\partial z'}\right) =$$

$$-\frac{\rho U^2}{L}\frac{\partial p'}{\partial x'}+\mu\left(\frac{U}{L^2}\frac{\partial^2 u'}{\partial x'^2}+\frac{U}{L^2}\frac{\partial^2 u'}{\partial y'^2}+\frac{U}{h^2}\frac{\partial^2 u'}{\partial z'^2}\right)+\frac{\mu}{3}\left(\frac{U}{L^2}\frac{\partial^2 u'}{\partial x'^2}+\frac{U}{L^2}\frac{\partial^2 v'}{\partial x'\partial y'}+\frac{U}{Lh}\frac{\partial^2 w'}{\partial z'^2}\right)$$

$$\frac{\rho U^2}{L}\left(\frac{du''}{dt}+u'\frac{\partial u'}{\partial x'}+v'\frac{\partial u'}{\partial y'}+w'\frac{\partial u'}{\partial z'}\right)=-\frac{\rho U^2}{L}\frac{\partial p'}{\partial x'}+\frac{\mu U}{L^2}\left(\frac{\partial^2 u'}{\partial x'^2}+\frac{\partial^2 u'}{\partial y'^2}+\frac{L^2}{h^2}\frac{\partial^2 u'}{\partial z'^2}\right)$$
$$+\frac{\mu U}{3L^2}\left(\frac{\partial^2 u'}{\partial x'^2}+\frac{\partial^2 v'}{\partial x'\partial y'}+\frac{L}{h}\frac{\partial^2 w'}{dx'\partial z'^2}\right)$$

The velocity in the z-direction, w, is assumed to be zero. Thus, the equation further reduces to

$$\left(\frac{du'}{dt'}+u'\frac{du'}{dx'}+v'\frac{du'}{dy'}\right)+\frac{\partial p'}{\partial x'}=\frac{1}{\mathrm{Re}}\left(\frac{\partial^2 u'}{\partial x'^2}+\frac{\partial^2 u'}{\partial y'^2}+\frac{L^2}{h^2}\frac{\partial^2 u'}{\partial z'^2}+\frac{1}{3}\frac{\partial^2 u'}{\partial x'^2}+\frac{1}{3}\frac{\partial^2 v'}{\partial x'\partial y'}\right).$$

By inspection, it can be seen that the terms on the right side of the equation are of order 1, 1, L^2/h^2, 1/3, and 1/3, respectively. For the current geometry, $L \geq 10h$, making the third term of order 100, or higher. From this, it can be assumed that the effects of the other four terms will be negligible when compared to the third term, resulting in the reduction

$$\left(\frac{du'}{dt'}+u'\frac{\partial u'}{\partial x'}+v'\frac{\partial u'}{\partial y'}\right)+\frac{\partial p'}{\partial x'}=\frac{1}{\mathrm{Re}}\frac{L^2}{h^2}\frac{\partial^2 u'}{\partial z'^2}$$

Re-dimensionalizing the above equation yields

$$\frac{L}{U^2}\frac{du}{dt}+\frac{L}{U^2}u\frac{\partial u}{\partial x}+\frac{L}{U^2}v\frac{\partial u}{\partial y}+\frac{L}{\rho U^2}\frac{\partial p}{\partial x}=\frac{\mu}{\rho U L}\frac{h^2}{U}\frac{L^2}{h^2}\frac{\partial^2 u}{\partial z^2}.$$

$$\rho\left(\frac{du}{dt}+u\frac{\partial u}{\partial x}+v\frac{\partial u}{\partial y}\right)+\frac{\partial p}{\partial x}=\mu\frac{\partial^2 u}{\partial z^2}$$

The resulting equation defines the x-component of the fluid flow field for the specified geometry. The y-component of the flow field is given by

$$\rho\left(\frac{dv}{dt}+u\frac{\partial v}{\partial x}+v\frac{\partial v}{\partial y}\right)+\frac{\partial p}{\partial y}=\mu\frac{\partial^2 v}{\partial z^2}$$

Also, since $\mathrm{Re} \ll 1$ and $\mathrm{Re} \approx \frac{\rho\vec{V}\left(\nabla\vec{V}\right)}{\mu\nabla^2\vec{V}} \approx \frac{\rho u\frac{\partial u}{\partial x}}{\mu\frac{\partial^2 u}{\partial z^2}}$, these equations further reduce to

$$\rho\frac{du}{dt}+\frac{\partial p}{\partial x}=\mu\frac{\partial^2 u}{\partial z^2}$$
$$\rho\frac{dv}{dt}+\frac{\partial p}{\partial y}=\mu\frac{\partial^2 v}{\partial z^2}.$$

The governing PDE for the fluid flow system then becomes

$$\frac{h^2}{6\mu}\left[\frac{\partial}{\partial x}\left(\tilde{\rho}\frac{\partial P}{\partial x}\right)+\frac{\partial}{\partial y}\left(\tilde{\rho}\frac{\partial P}{\partial y}\right)\right]=\frac{\partial\left(\tilde{\rho}U\right)}{\partial x}+\frac{\partial\left(\tilde{\rho}V\right)}{\partial y},$$

where P is the pressure, x is the distance from the center of the disc along the x-axis, y is the distance from the center of the oscillating disc along the y-axis, $\rho=\tilde{\rho}(x,y)e^{i\omega t}$, and fluid velocity at $z=h$ will be $u=U(x,y)e^{i\omega t}$ and $v=V(x,y)e^{i\omega t}$.

REFERENCES

[1] Bao, M., Yang, H., Yin, H., and Sun, Y., "Energy transfer model for squeeze–film air damping in low vacuum," *Journal of Micromechanics and Microengineering*, vol. 12, pp. 341–6, 2002.

[2] Bao, M.-H., *Micromechanical transducers : pressure sensors, accelerometers and gyroscopes*, vol. 8 of *Handbook of sensors & actuators*. Amsterdam: Elsevier Science, 2000.

[3] Bird, G. A., *Molecular gas dynamics and the direct simulation of gas flows*. New York: Clarendon Press, 1994.

[4] Blech, J. J., "On isothermal squeeze films," *Journal of Lubrication Technology*, vol. 105, pp. 615–20, 1983.

[5] Cho, Y. H., Pisano, A. P., and Howe, R. T., "Viscous damping model for laterally oscillating microstructures," *Journal of Microelectromechanical Systems*, vol. 3, no. 2, pp. 81–7, 1994.

[6] Christian, R. G., "The theory of oscillating-vane vacuum gauges," *Vacuum*, vol. 16, no. 4, pp. 175–8, 1966.

[7] Corporation, S. P., "Microelectromechanical systems (mems), an spc market study," January, 1999.

[8] el Hak, M. G., "The fluid mechanics of microdevices-the freeman scholar lecture," *J. Fluids Engineering*, vol. 121, pp. 5–33, 1999.

[9] el Hak, M. G., *The MEMS handbook*. Boca Raton, FL: CRC Press., 2002.

[10] Goodman, F. O. and Wachman, H. Y., *Dynamics of Gas-Surface Scattering*. New York: Academic Press, 1976.

[11] Hadjiconstantinou, N. G., "Sound wave propagation in transition-regime micro- and nanochannels," *Physics of Fluids*, vol. 14, no. 2, pp. 802–9, 2002.

[12] Hadjiconstantinou, N. G. and Garcia, A. L., "Molecular simulations of sound wave propagation in simple gases," *Physics of Fluids*, vol. 13, no. 4, pp. 1040–6, 2001.

[13] Halliday, D., Resnick, R., and Walker, J., *Fundamentals of Physics: Extended*, pp. 484–501. New York: John Wiley and Sons, fifth ed., 1997.

[14] Hosaka, H., Itao, K., and Kuroda, S., "Damping characteristics of beam-shaped micro-oscillators," *Sensors and Actuators A*, vol. 49, pp. 87–95, 1995.

[15] Hughes, W. F. and Brighton, J. A., *Schaum's Outline of Theory and Problems of Fluid Dynamics*. Schaum's Outline, New York: McGraw-Hill, 3rd ed., 1999.

[16] Kadar, Z., Kindt, W., Bossche, A., and Mollinger, J., "Quality factor of torsional resonators in the low-pressure region," *Sensors and Actuators A*, vol. 53, pp. 299–303, 1996.

[17] Langlois, W. E., "Isothermal squeeze films," *Quarterly Applied Mathematics*, vol. XX, no. 2, pp. 131–50, 1962.

[18] Li, B., Wu, H., Zhu, C., and Liu, J., "The theoretical analysis on damping characteristics of resonant microbeam in vacuum," *Sensors and Actuators A*, vol. 77, pp. 191–4, 1999.

[19] Lifshitz, R. and Roukes, M. L., "Thermoelastic damping in micro- and nanomechanical systems," *Phys. Rev. B*, vol. 61, no. 8, pp. 5600–9, 2000.

[20] Melvas, P., Kalvesten, E., and Stemme, G., "A surface-micromachined resonant-beam pressure-sensing structure," *Journal of Microelectromechanical Systems*, vol. 10, no. 4, pp. 498–502, 2001.

[21] Mihailovich, R. E. and MacDonald, N. C., "Dissipation measurements of vacuum-operated single-crystal silicon microresonators," *Sensors and Actuators A*, vol. 50, pp. 199–207, 1995.

[22] Newell, W. E., "Miniaturization of tuning forks," *Science*, vol. 161, pp. 1320–6, 1968.

[23] Paton, R. L., *Incompressible Flow*. The Mechanical engineering handbook series, New York: Wiley-Interscience, second edition ed., 1996.

[24] Pourkamali, S., Hashimura, A., Abdolvand, R., Ho, G. K., Erbil, A., and F, F. A., "High-q single crystal silicon harpass capacitive beam resonators with self-aligned sub-100-nm transduction gaps," *Journal of Microelectromechanical Systems*, vol. 12, no. 4, pp. 487–96, 2003.

[25] Schaaf, S. A. and Chambre, P. L., *Flow of Rarefied Gases*. Princeton: Princeton University Press, 1961.

[26] Senturia, S. D., *Microsystem Design*. Boston: Kluwer Academic Publishers, 2001.

[27] Sharipov, F., Marques, W., Jr., and Kremer, G. M., "Free molecular sound propagation," *The Journal of the Acoustical Society of America*, vol. 112, no. 2, pp. 395–401, 2002.

[28] Starr, J. B., "Squeeze film damping in solid-state accelerometers," in *Tech. Digest, IEEE Solid State Sensor and Actuator Workshop*, (Hilton Head Island, SC), pp. 44–47, IEEE, June 1990.

[29] Veijola, T., Kuisma, H., and Lahdenper, J., "The influence of gas-surface interaction on gas-film damping in a silicon accelerometer," *Sensors and Actuators A: Physical*, vol. 66, pp. 83–92, 1998.

[30] Veijola, T. and Turowski, M., "Compact damping models for laterally moving microstructures with gas-rarefaction effects," *Journal of Microelectromechanical Systems*, vol. 10, no. 2, pp. 263–73, 2001.

[31] Wang, L.-P., R. Wolf, J., Wang, Y., Deng, K. K., Zhou, L., Davis, R. J., and Trolier-McKinstry, S., "Design, fabrication, and measurement of high-sensitivity piezoelectric microelectromechanical systems accelerometers," *Journal of Micromechanics and Microengineering*, vol. 12, no. 4, pp. 433–9, 2003.

[32] Weisstein, E. W., "Navier-stokes equations." `http://scienceworld.wolfram.com/physics/Navier-StokesEquations.html`.

[33] Yasumura, K. Y., Stowe, T. D., Chow, E. M., Pfafman, T., Kenny, T. W., D., B. C. S., and Rugar, "Quality factors in micron- and submicron-thick cantilevers," *Journal of Microelectromechanical Systems*, vol. 9, no. 1, pp. 117–25, 2000.

[34] Ye, W., Wang, X., Hemmert, W., Freeman, D., and White, J., "Air damping in lateral oscillating micro resonators: a numerical and experimental study," *Journal of Microelectromechanical Systems*, vol. 12, no. 5, pp. 557–66, 2003.

[35] Zhang, C., Xu, G., and Jiang, Q., "Characterization of the squeeze film damping effect on the quality factor of a microbeam resonator," *Journal of Micromechanics and Microengineering*, vol. 14, no. 10, pp. 1302–6, 2004.

[36] Zhou, J., Li, P., Zhang, S., Zhou, F., Huang, Y., Yang, P., and Bao, M., "A novel mems gas sensor with effective combination of high sensitivity and high selectivity," in *Proc. of the 13th IEEE Int. Symp. on Applications of Ferroelectrics, ISAF 2002*, pp. 471–4, ISAF, 2002.

[37] Zook, J. D., Burns, D. W., Guckel, H., Sniegowski, J. J., Engelstad, R. L., and Z, F., "Characteristics of polysilicon resonant microbeams," *Sensors and Actuators A*, vol. 35, pp. 51–9, 1992.